

# Locally Balanced Dendritic Integration by Short-Term Synaptic Plasticity and Active Dendritic Conductances

Vladislav Volman,<sup>1,2</sup> Herbert Levine,<sup>1</sup> Eshel Ben-Jacob,<sup>1,3</sup> and Terrence J. Sejnowski<sup>1,2,4</sup>

<sup>1</sup>Center for Theoretical Biological Physics, University of California at San Diego, La Jolla, California; <sup>2</sup>Howard Hughes Medical Institute, Computational Neurobiology Laboratory at The Salk Institute for Biological Studies, La Jolla, California; <sup>3</sup>School of Physics and Astronomy, Tel-Aviv University, Tel-Aviv, Israel; and <sup>4</sup>Division of Biological Sciences, University of California at San Diego, La Jolla, California

Submitted 24 March 2009; accepted in final form 10 September 2009

**Volman V, Levine H, Ben-Jacob E, Sejnowski TJ.** Locally balanced dendritic integration by short-term synaptic plasticity and active dendritic conductances. *J Neurophysiol* 102: 3234–3250, 2009. First published September 16, 2009; doi:10.1152/jn.00260.2009. The high degree of variability observed in spike trains and membrane potentials of pyramidal neurons *in vivo* is thought to be a consequence of a balance between excitatory and inhibitory inputs, which depends on the dynamics of the network. We simulated synaptic currents and ion channels in a reconstructed hippocampal CA1 pyramidal cell and show here that a local balance can be achieved on a dendritic branch with a different mechanism, based on presynaptic depression of quantal release interacting with active dendritic conductances. This mechanism, which does not require synaptic inhibition, allows each dendritic branch to remain sensitive to correlated synaptic inputs, induces a high degree of variability in the output spike train, and can be combined with other balance mechanisms based on network dynamics. This hypothesis makes a testable prediction for the cause of the observed variability in the firing of hippocampal place cells.

## INTRODUCTION

There is a maintained, but low level of spontaneous activity in cortical and hippocampal neurons *in vivo*, characterized by highly irregular spike trains (Csicsvari et al. 1999). Both the pyramidal neurons and the local inhibitory interneurons increase their firing rates in response to a strong excitatory input, but the variability in the spike trains remains high (Csicsvari et al. 1999; Fenton and Muller 1998; Muller et al. 1987). This is inconsistent with the naïve picture of a neural integrator driven by a large number of small postsynaptic potentials, in which variability is proportional to  $1/\sqrt{N_s}$ , where  $N_s$  is the number of synaptic events that are needed to cross the threshold for spike generation (Softky and Koch 1993). One possible explanation for this high variability in hippocampal neurons activity is that, in analogy to cortical neurons, both the excitatory and inhibitory inputs to the pyramidal neurons increase in such a way that balance is maintained, with the increase in spike rate a consequence of the increased variance of the membrane potential. This explanation depends on a close match between the excitatory and inhibitory inputs within the recurrent networks (Salinas and Sejnowski 2000; Shadlen and Newsome 1998), a condition that might not necessarily be precisely fulfilled in hippocampal CA1 pyramidal neurons (Csicsvari et al. 1999).

An alternate mechanism by which the balance of activity within a neuron could be maintained is through local mechanisms at excitatory synapses that do not depend on the presence of local inhibition. Short-term synaptic depression occurs at these synapses, which could reduce the excitatory drive and introduce variability and correlations in release patterns of synaptic neurotransmitter (Zucker and Regehr 2002). On the postsynaptic side of the synapse, hyperpolarizing conductances such as  $\text{Ca}^{2+}$ -activated  $\text{K}^+$  currents that affect spike initiation will also affect the variability of spike times (Larkum and Nevian 2008; Magee and Cook 2000; Stuart et al. 1999). Both of these mechanisms have been studied separately in previous modeling studies (Abbott et al. 1997; de la Rocha and Parga 2005), but there has been no discussion of the consequences of their interaction on the variability of spike timing.

Here, we used a biophysically realistic model of excitatory Schaffer collateral synapses on a reconstructed CA1 hippocampal neuron and compartmental modeling techniques to investigate local balance in dendrites induced by short-term presynaptic plasticity in the quantal model of synaptic transmission. We found that notwithstanding the large number of excitatory synaptic inputs, the output spike trains were highly irregular. Short-term depression interacted with the slow afterhyperpolarizing  $\text{Ca}^{2+}$ -activated  $\text{K}^+$  currents present in dendrites to maintain a high degree of spiking variability over a wide range of excitatory drive. This mechanism, which does not depend on previously proposed concepts such as shunting inhibition or excitation-inhibition balance, produced a robust balance within each dendritic branch. Finally, we used the model to explain the variability observed in place cells in the rat hippocampus during active exploration (Fenton and Muller 1998), which led to a testable prediction for the how spike number variability could be maintained in CA1 pyramidal cells.

## METHODS

### *Stochastic synaptic transmission*

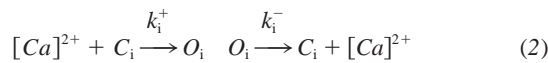
The question of how presynaptic mechanisms interact with postsynaptic mechanisms depends on the biophysical properties of synaptic release at terminals. The synaptic model used here is an extended version of Bertram-Sherman-Stanley (BSS) model (Bertram et al. 1996; Nadkarni and Jung 2007), which provides a relatively simple, yet biophysically realistic framework for modeling of single-vesicle presynaptic short-term plasticity. According to the bound calcium hypothesis, the facilitation of release is caused by the slow unbinding rate of calcium. In the model, each active zone (release site) consists of four independently operating  $\text{Ca}^{2+}$  gates, and each gate has its own

Address for reprint requests and other correspondence: V. Volman, Ctr. for Theoretical Biological Physics, Univ. of California at San Diego, La Jolla, CA 92093 (E-mail: volman@salk.edu).

rate of binding/unbinding calcium. The rates of gates opening are nearly the same (Table 1), but the rates of closing span several orders of magnitude, allowing for short-time facilitation to be manifested as a slow unbinding of  $Ca^{2+}$  from the slowest gate. If at least one vesicle is available, a quantum of neurotransmitter is released with probability

$$p_{\text{release}} = O_1 \times O_2 \times O_3 \times O_4 \tag{1}$$

where for the  $i$ th gate ( $i = 1, 2, 3, 4$ ), the probability of open state occupancy  $O_i$  and the probability of closed state occupancy  $C_i$  are determined by the kinetic equations (Bertram et al. 1996)



The probability of releasing a vesicle on stimulation depends on the amount of calcium influx during action potential (AP). The calcium signal at the presynaptic terminal after the arrival of the AP is described as a two-step process of exponential growth with a time constant  $\tau_{\text{rise}} = 50 \mu\text{s}$ , followed by an exponential decay with the time constant  $\tau_{\text{fall}} = 1 \text{ ms}$ . This level of modeling accounts both for calcium influx to the synaptic terminal via voltage-gated calcium channels (rise part) and for the fast internal buffering and extrusion of calcium from the presynaptic terminal (fall part). After the vesicle has fused with the membrane and released neurotransmitter, the synapse enters a short “refractory” phase during which further fusion is not possible (Dobrunz et al. 1997). This process is modeled here by assuming that no vesicle is released from the given presynaptic terminal during  $\Delta T_{\text{ref}} = 5 \text{ ms}$  after a successful fusion of vesicle at that same terminal. After the refractory period, the calcium signal at the presynaptic terminal has decayed; although in principle the model allows for asynchronous release of neurotransmitter to occur, in practice, the probability is quite low, unless there is residual presynaptic calcium.

The BSS model describes the release process, but it makes no assumptions about the number and availability of vesicles. CA3–CA1 synapses are known to have a relatively small number of vesicles in the readily releasable pool (RRP) (Dobrunz and Stevens 1997). For clarity of presentation and ease in interpreting the results, we assume, unless specifically indicated otherwise, that the maximal number of docked vesicles,  $n_{\text{ves}}$ , at each model synapse is  $n_{\text{ves}} = 5$ . Furthermore, we adopt the uni-vesicular release hypothesis, by which at most one vesicle from the given presynaptic terminal can be fused during a successful release event (Dobrunz and Stevens 1997). After being released, a new vesicle becomes available for release with probability  $dt/\tau_r$ , where  $\tau_r$  is the time constant of RRP replenishment. The rate with which RRP is replenished had been estimated to vary from  $0.1 \text{ s}^{-1}$  to  $0.5 \text{ s}^{-1}$ , depending on experimental conditions (such as extracellular calcium concentration) and history of synaptic activity (Dobrunz and Stevens 1997; Garcia-Perez and Wesseling 2008; Stevens and Tsujimoto 1995). In addition, calcium-induced augmentation can effectively mask slow stochastic recovery, thus leading to a very fast, step-like, rebound from depression (Garcia-Perez and Wesseling 2008). In the model, unless otherwise indicated, we assumed that, after a successful fusion, a vesicle becomes unavailable for  $\Delta T_{\text{R}} = 2 \text{ s}$ . This assumption represents an approximation of

biological stochastic recovery process, yet it allows us to significantly reduce the computational load associated with explicit modeling of many stochastic processes. The general validity of our conclusions (high variability of spiking for model neurons with active dendrites vs. relatively low variability of spiking for model neurons with passive dendrites) was tested in preliminary simulations that used the model with stochastic ( $\tau_r = 5 \text{ s}$ ) replenishment of the RRP.

This model of stochastic synaptic transmission at CA3–CA1 synapses captures both synaptic short-term facilitation and short-term depression. Facilitation of release probability occurs because of the slow unbinding of  $Ca^{2+}$  ions from the calcium gates at the presynaptic active zone (Bertram et al. 1996). Depression of synaptic response is prominent for high stimulation frequencies because each release zone possesses only a finite number of docked vesicles (Dobrunz and Stevens 1997). This model of facilitation/depression is in accordance with known biophysical mechanisms underlying these two phenomena (Zucker and Regehr 2002). A completely deterministic synapse (reliably releasing quantum of transmitter following each incoming AP), stimulated with uncorrelated Poisson spike-trains at rate  $\nu$ , depresses for  $\nu > n_{\text{ves}}/\tau_r$ . However, in a model of activity-dependent stochastic release, the frequency  $n_{\text{ves}}/\tau_r$  can only be considered as a lowest frequency above which stochasticity and correlations can lead to nontrivial variability of release.

### Cell characteristics

Because the interactions between ionic currents within a dendritic branch depend on the spatial organization of the dendrites, we used the morphology of a reconstructed CA1 pyramidal neuron (cell c20466, available at [www.neuromorpho.org](http://www.neuromorpho.org)) (Ishizuka et al. 1995). This cell had the following characteristics: the surface area of the entire dendritic tree was  $23,162 \mu\text{m}^2$ ; the surface area of the soma was  $358 \mu\text{m}^2$ ; the surface area of entire main trunk was  $6,089 \mu\text{m}^2$ ; and the surface area of the proximal portion of the apical dendrite (1st 350  $\mu\text{m}$  from soma) was  $1,500 \mu\text{m}^2$ . In proximal apical dendrites of CA1 pyramidal neurons, there was one synaptic terminal per spine, and the spine density was  $\sim 0.5 \text{ spines}/\mu\text{m}$  (Andersen et al. 2007). In the computational model,  $10^3$  synapses were distributed over the branches of proximal apical dendrites in the following way. First, a random branch was picked with probability proportional to its length. Then, the location of synaptic terminal within the branch was determined. This procedure (of length-biased branch selection) ensured that the density of model synaptic terminals would be the same in long and short branches. However, because of the compartmental approximation, the actual number of synapses per micron fluctuated, as shown in Fig. 1F. To account for the presence of spines, the surface area of dendritic tree was increased, assuming individual spine area of  $0.28 \mu\text{m}^2$  and uniform density of  $0.5 \text{ spines}/\mu\text{m}$  (Harris et al. 1992; Maletic-Savatic et al. 1999).

### Specification of channel composition

Dendritic trees of CA1 pyramidal neurons possess a variety of active dendritic conductances, which are often nonuniformly distributed along the tree and can display activation/inactivation on a variety of time scales (Magee and Johnston 1995; Mainen and Sejnowski 1998; Migliore and Shepherd 2002). Here, we used standard compartmental modeling techniques to simulate dynamics of reconstructed CA1 pyramidal neurons with biophysically realistic passive and active properties.

The model incorporated several types of voltage-gated currents: a fast  $Na^+$  current,  $I_{Na}$  (Magee and Johnston 1995; Migliore et al. 2005); a noninactivating delayed rectifier  $K^+$  current,  $I_{Kdr}$  (Hoffman et al. 1997; Migliore et al. 1999); a transient A-type  $K^+$  current,  $I_{Ka}$  (Hoffman et al. 1997; Migliore et al. 1999); a slow, noninactivating  $K^+$  current,  $I_{Ksm}$  (Mainen and Sejnowski 1998); a nonspecific hyperpolarization-activated cation current,  $I_h$  (Lorincz et al. 2002; Magee 1998; Migliore et al. 2005; Poolos et al. 2002); and a slow  $Ca^{2+}$ -activated afterhyperpolarization

TABLE 1. Rates of calcium binding and unbinding for different gates in Bertram-Sherman-Stanley model of synaptic transmitter release

Binding Rate, $\mu\text{M}/\text{ms}$	Unbinding Rate, $\text{ms}^{-1}$
$k_1^+ = 3.75 \cdot 10^{-3}$	$k_1^- = 4 \cdot 10^{-4}$
$k_2^+ = 2.5 \cdot 10^{-3}$	$k_2^- = 10^{-3}$
$k_3^+ = 5 \cdot 10^{-4}$	$k_3^- = 0.1$
$k_4^+ = 7.5 \cdot 10^{-3}$	$k_4^- = 10$

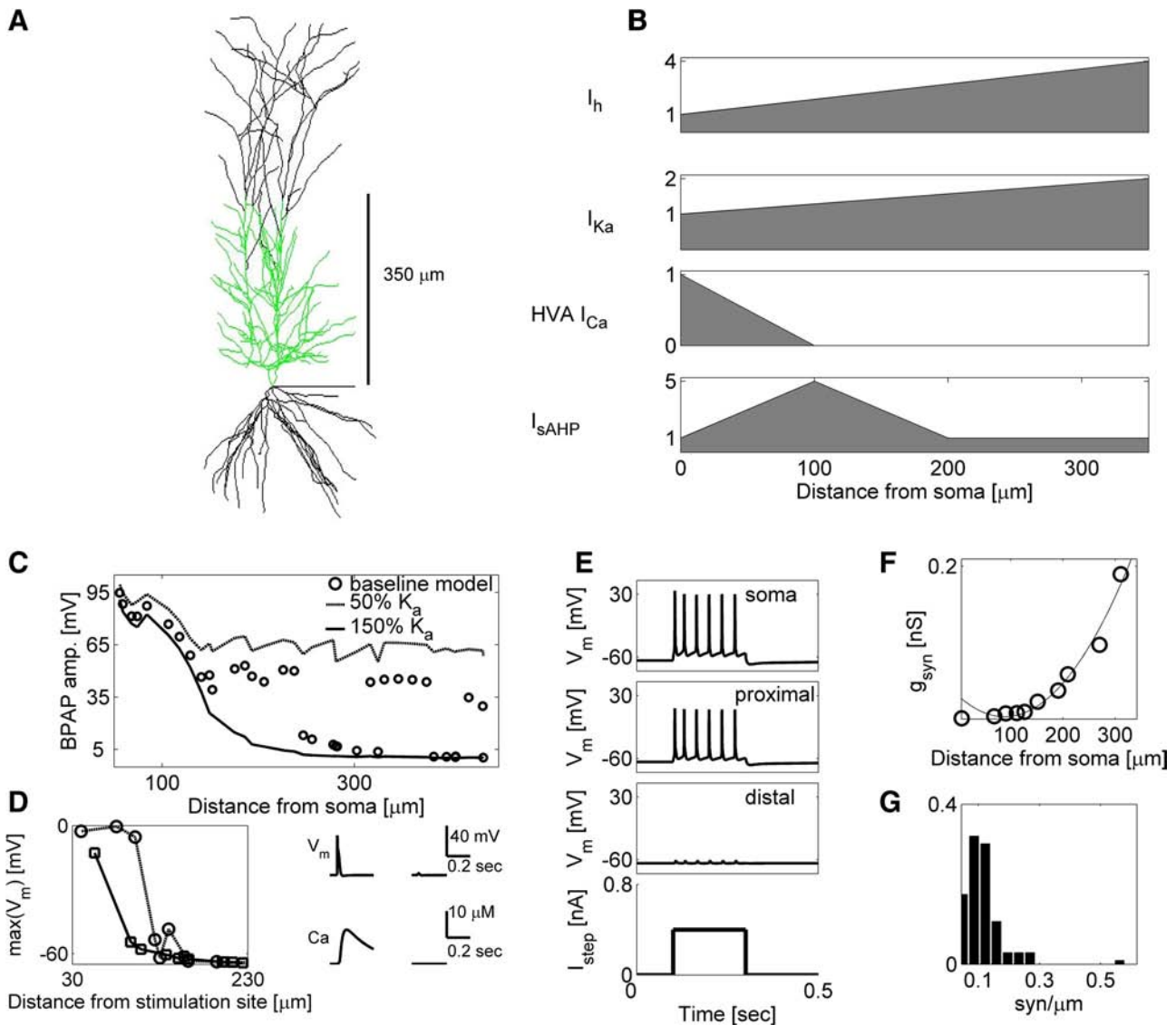


FIG. 1. CA1 pyramidal cell model. *A*: the reconstructed dendritic tree of a CA1 pyramidal neuron. Model synapses were distributed only on the proximal 350  $\mu\text{m}$  of the apical dendrite (bright region) to mimic Schaffer collateral inputs. *B*: spatially nonuniform distributions of active conductances in the dendritic tree. Conductance values scaled relative to values at soma. *C*: action potential (AP) back-propagation into dendritic tree. Amplitude as a function of distance from the soma for different values of maximal dendritic A-type potassium channel conductance. Circles, baseline model; solid line, model with  $\bar{g}_{K_a}$  scaled by 1.5; dashed line, model with  $\bar{g}_{K_a}$  scaled by 0.5. *D*: the extent of dendritic spike propagation, measured as the maximal membrane potential in dendritic compartments that neighbored the stimulated compartment. Dendritic spikes propagated for a typical distance of 80  $\mu\text{m}$  and could evoke significant changes in local dendritic calcium concentration. Shown are examples for 2 different apical dendritic compartments. *Right*: examples of membrane voltage and calcium concentration in the stimulated dendritic compartment (*left*) and the compartment that is distal to the stimulated one (*right*). *E*: an example of back-propagating APs elicited by a current step applied to somatic compartment. Back propagating action potentials (BPAPs) reliably propagated to proximal but not to distal apical dendritic compartments (see *C*). *F*: scaling of synaptic conductance with the distance from soma (circles) and the best quadratic fit (solid line):  $y = 10^{-2} \times (a + bx + cx^2)$  nS, with  $a = 3.7981$ ,  $b = -0.0583$ , and  $c = 3.318 \times 10^{-4}$ . *G*: distribution of linear synaptic density (number of synapses in the branch per branch length).

(AHP)  $K^+$  current,  $I_K^{\text{sAHP}}$  (Mainen and Sejnowski 1998; Poirazi et al. 2003a). Activation properties of the A-type  $K^+$  current in the dendrites of CA1 pyramidal neurons were dependent on location:  $I_{K_a}$  activation in distal dendrites was hyperpolarized by 12 mV compared with the voltage dependence in the soma and proximal dendrites (Hoffman et al. 1997). Activation/inactivation curves and time constants of activation/inactivation variables of different channels that we used are provided in Supplementary Materials.<sup>1</sup>

Calcium excitability was accounted for by incorporating two types of  $\text{Ca}^{2+}$  currents: a high-voltage activated L-type  $\text{Ca}^{2+}$  current,  $I_{\text{Ca}}^{\text{HVA}}$  (Mainen and Sejnowski 1998; Poirazi et al. 2003a; Westenbroek et al. 1990), and voltage-activated R-type  $\text{Ca}^{2+}$  current,  $I_{\text{Ca}}^{\text{R}}$  (Mainen and

Sejnowski 1998; Poirazi et al. 2003a). Calcium extrusion was modeled as a linear process with the equilibrium level of  $c_s = 0.1 \mu\text{M}$  and an extrusion time constant of  $\tau_{\text{Ca}} = 200$  ms (Poirazi et al. 2003a)

$$\frac{d[\text{Ca}^{2+}]_i}{dt} = \frac{c_s - [\text{Ca}^{2+}]_i}{\tau_{\text{Ca}}} \quad (3)$$

Diffusion and buffering of calcium ions were not incorporated into the model for the following reasons: First, Schaffer collaterals in pyramidal neurons project onto dendritic spines, which act as chemical compartments, allowing localized dynamics of  $[\text{Ca}^{2+}]_i$  that does not, or very weakly, affect nearby synaptic terminals (Yuste and Denk 1995). Moreover, even in aspiny synapses, dendritic calcium transients evoked by quantal release of synaptic transmitter are usually

<sup>1</sup> The online version of this article contains supplemental data.

localized because of the action of calcium buffers (Murthy et al. 2000). Nonetheless, intense synaptic stimulation could produce calcium-mediated cross-talk between adjacent synapses; however, the presynaptic depression in the model significantly reduced the possibility that persistent stimulation could lead to persistent synaptic release. We therefore did not include dendritic calcium diffusion and buffering in the model, which would have significantly increased the computational complexity of the simulations.

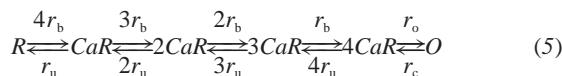
In most of the simulations, we used a standard model of the slow, apamine-insensitive, AHP currents in CA1 pyramidal neurons (Poirazi et al. 2003a), which assumes that the activation variable of the slow AHP (sAHP) channel is a direct function of calcium concentration. In this model, the “slowness” of sAHP is primarily determined by the time-course of calcium transient. Because the identity of the potassium channel underlying the sAHP in hippocampal pyramidal neurons is still unknown, we assessed the general validity of our results by performing preliminary simulations with two additional models of the sAHP.

In the first model (Traub et al. 2003), the evolution of the fraction of open sAHP channels,  $m$ , was described by the differential equation

$$\frac{dm}{dt} = \alpha \times [Ca^{2+}] \times (1 - m) - \frac{m}{\tau_m} \tag{4}$$

with  $\alpha = 20/s/mM$  and  $\tau_m = 1$  s. Compared with our baseline model of sAHP, the decay of adaptation here was not dependent on calcium concentration and was much slower.

Another, more detailed, model of sAHP described the activation of calcium-dependent potassium channel as a four-stage stochastic process (Sah and Clements 1999)



Following Sah and Clements (1999), the reaction rates here were  $r_b = 10 \mu M/s$ ,  $r_u = 0.5/s$ ,  $r_o = 600/s$ ,  $r_c = 400/s$ .

In some simulations (Fig. 4), active conductances were removed from dendritic compartments to test the transfer properties of a model neuron with a passive dendritic tree. Removal of active conductances resulted in an increase in neuronal firing rate. To make the firing rate of the passive model neuron comparable to its firing rate in at least some of the active conductances scenarios, the membrane resistivity in dendritic compartments was reduced twofold to  $R_m = 14 K\Omega \cdot cm^2$ .

*Spatial distribution of active mechanisms*

Active conductances are often nonuniformly distributed throughout the dendritic structure. This property is crucial for the information-processing capabilities of the dendritic tree, because it enables the neuron to distinguish between different spatio-temporal input patterns and thus can serve as a cellular level implementation of pattern recognition (Reyes 2001; Williams and Stuart 2003). Based on the existing experimental observations, a CA1 pyramidal neuron was modeled with realistic distributions of active conductances (Tables 2 and 3; Fig. 1, A and B, for spatially nonuniformly distributed conductances; Supplementary Figures for all conductances). The resulting model of CA1 pyramidal neuron exhibited some of the well-known features of real neurons. For example, somatic step-like current stimulation generated

TABLE 2. Parameter values for passive dendritic properties used in the model

Membrane capacitance	$C$	$1 \mu F/cm^2$
Membrane resting voltage	$E_{rest}$	$-65$ mV
Axial resistivity	$R_{axial}$	$180 \Omega \cdot cm$
Surface resistivity	$R_{membrane}$	$28 K\Omega \cdot cm^2$

TABLE 3. Values of active conductances that have been used in modeling of somatic and axonal compartments

Active Conductance	Soma	Axon
$g_{Na}$	200	400
$g_{Kdr}$	100	100
$g_{Ka}$	250	250
$g_{Km}$	0.1	—
$g_{sAHP}$	1.0	—
$g_{lh}$	0.5	—
$g_{Ca}^{HVA}$	12	—
$g_{Ca}^R$	15	—

All conductances are given in  $pS/\mu m^2$ .

back-propagating APs that could reach proximal apical, but not distal, dendrites, and the extent of back propagating action potential (BPAP) invasion into dendritic tree could be controlled by the level of dendritic A-type potassium conductance (Fig. 1, C and E) (Golding et al. 2001). The model neuron also supported local dendritic sodium spikes that could spread to a limited distance ( $\sim 80 \mu m$ ) from the site of stimulation (Fig. 1D).

*Synaptic conductance and synapse density*

In apical dendrites of CA1 pyramidal neurons, the electrotonic decay of the postsynaptic response is partially compensated by increased synaptic conductance. As a result, somatic excitatory postsynaptic potential (EPSP) peak value is approximately independent of synaptic location, because the local EPSP amplitude increases as nearly a quadratic function of distance from the soma (Magee and Cook 2000). The exact quantitative relation between the height of synaptic conductance and its distance from the soma is, of course, unique to a specific neuron, and depends on the details of neuronal morphology, as well as on the distribution of its passive and active mechanisms. To recover this relation, we positioned model synapse at progressively increasing distances from the soma, and tuned the values of local synaptic conductances to yield 0.2 mV somatic depolarization on synaptic stimulation (assuming that presynaptic stimulation reliably leads to transmitter release) (Li and Ascoli 2006). The resulting set of (distance, weight) points were fitted with a second-degree polynomial function.

The set of weights as a function of distance from the soma is shown in Fig. 1E. The values of synaptic conductances on the apical dendrites varied from  $\sim 50 pS/\mu m^2$  (for synapses proximal to soma) to  $\sim 300 pS/\mu m^2$  (for synapses further away from soma). Assuming postsynaptic density area  $\approx 1 \mu m^2$  and  $\Delta V \approx 60$  mV, the magnitude of the synaptic currents are  $I_{AMPA} \approx 3-18$  pA. This range of values is consistent with the measured values of average synaptic potency for CA3-CA1 synapses ( $14 \pm 7$  pA) (Dobrunz and Stevens 1997).

*Analysis of neuronal gain and spike time-series variability*

Neuronal gain is defined as a ratio of neuronal firing rate (output) to input rate, and gain modulation refers to the changes in the functional relation between input and output rates.

As a measure of output spiking activity, we used the averaged instantaneous output rate, defined as  $(ISI^{-1})$ , with the averaging performed over all interspike intervals (ISIs) in the spike train. This measure becomes identical to the mean rate in the limit of a regular spike train.

The variability of spike time series is usually assessed using the  $CV = \sigma(ISI)/\mu(ISI)$  of ISI series (Gabbiani and Koch 1998); however, as noted elsewhere (Gabbiani and Koch 1998; Holt et al. 1996), the CV fails to provide an accurate estimate of ISI variability when the mean firing rate of a neuron changes over time. As we show later, this is exactly what happens in our model of the CA1 pyramidal neuron driven by a large number of stochastic inputs arriving from plastic

synaptic terminals. Variability in the spiking activity of this cell might arise from transient rate adaptation (because of the activation of sAHP conductance) or as a result of intermittent periods of silence during which most of the synaptic neurotransmitter vesicles are not being released. We used here an alternative measure, devised to specifically overcome the undesirable effect of a slowly modulated firing rate (Holt et al. 1996). This measure is defined as

$$CV_2 = 2 \cdot \left\langle \frac{|ISI_{i+1} - ISI_i|}{ISI_{i+1} + ISI_i} \right\rangle \quad (6)$$

where the average is taken over all pairs of consecutive ISIs. The case  $CV_2 = 0$  corresponds to a completely regular spike train, and it can be shown (Holt et al. 1996) that for a spike train described by the Poisson process,  $CV_2$  is equal to 1 (as is the CV).

To provide the connection between membrane voltage trajectories and the observed variability in spike time series, we used the framework developed by Troyer and Miller (1997). In this view, the variability of spike time series is determined by the fraction of ISI that the neuron spends in the steady-state regimen (after complete recovery from postspike AHP). To compute the time of ISI settling in the steady state, we first computed the mean postspike membrane voltage trace by averaging over voltage trajectories of all ISIs. Next, the discrete derivative  $\frac{\Delta V}{\Delta t} = \frac{V(t + \Delta t) - V(t)}{\Delta t}$  of the mean postspike voltage was computed and smoothed by averaging over the running window (10–80 ms wide,  $\Delta t = 0.1$  ms). The first time (after the peak of postspike AHP) at which the smoothed  $\frac{\Delta V}{\Delta t}$  attained the value of zero was taken as the time of ISI settling in the steady-state regimen and also defined the duration of postspike AHP.

### Numerical simulations

All simulations were performed with the NEURON program (Hines and Carnevale 2001). Cable and synaptic dynamics were solved with the time step  $\Delta t = 10 \mu\text{s}$ . On a Linux workstation with a 2-GHz processor, 1 s of simulation took  $\sim 30$  min.

### Channel kinetics

We provide here the kinetics of all ionic currents that were used in our modeling of the CA1 pyramidal neuron (graphs of steady-state activation, inactivation, and time constants as a function of voltage are available in Supplementary Materials). In the following, time constants  $\tau_x$  are given in units of milliseconds, the voltage values are in units of millivolts, and current densities are in  $\mu\text{A}/\text{cm}^2$ . The indices used to designate activation/inactivation variables are described by different equations for different ionic current, e.g.,  $m_{\text{Na}} \neq m_{\text{K}}$ .

Sodium current:

$$I_{\text{Na}} = g_{\text{Na}} m^3 h (V - E_{\text{Na}}); E_{\text{Na}} = 55 \text{ mV}; \dot{m} = (m_{\infty} - m)/\tau_m;$$

$$\dot{h} = (h_{\infty} - h)/\tau_h$$

$$m_{\infty} = \alpha_m / (\alpha_m + \beta_m); \alpha_m = 0.4(V + 30) / \{1 - \exp[-(V + 30)/7.2]\}$$

$$\tau_m = 0.5 / (\alpha_m + \beta_m); \beta_m = 0.124(V + 30) / \{\exp[(V + 30)/7.2] - 1\}$$

$$h_{\infty} = 1 / \{1 + \exp[(V + 50)/4]\}; \alpha_h = 0.03(V + 45) / \{1 - \exp[-(V + 45)/1.5]\}$$

$$\tau_h = 0.5 / (\alpha_h + \beta_h); \beta_h = 0.01(V + 45) / \{\exp[(V + 45)/1.5] - 1\}$$

Delayed rectifier potassium current:

$$I_{\text{Kdr}} = g_{\text{Kdr}} m (V - E_{\text{K}}); E_{\text{K}} = -90 \text{ mV}; \dot{m} = (m_{\infty} - m)/\tau_m;$$

$$m_{\infty} = 1 / (1 + \alpha_m)$$

$$\tau_m = 50 \beta_m / (1 + \alpha_m); \alpha_m = \exp[-0.11(V - 13)];$$

$$\beta_m = \exp[-0.08(V - 13)]$$

A-type potassium current in proximal dendrites ( $\leq 100 \mu\text{m}$ ):

$$I_{\text{Ka}} = g_{\text{Ka}} m h (V - E_{\text{K}}); E_{\text{K}} = -90 \text{ mV}; \dot{m} = (m_{\infty} - m)/\tau_m;$$

$$\dot{h} = (h_{\infty} - h)/\tau_h$$

$$m_{\infty} = 1 / (1 + \alpha_m); \alpha_m = \exp[-0.038(1.5 + 1 / \{1 + \exp[(V + 40)/5]\})(V - 11)]$$

$$\tau_m = 4 \beta_m / (1 + \alpha_m); \beta_m = \exp[-0.038(0.825 + 1 / \{1 + \exp[(V + 40)/5]\})(V - 11)]$$

$$h_{\infty} = 1 / (1 + \alpha_h); \tau_h = 0.26(V + 50); \alpha_h = \exp[0.11(V + 56)]$$

A-type potassium current in distal dendrites ( $> 100 \mu\text{m}$ ):

$$I_{\text{Ka}} = g_{\text{Ka}} m h (V - E_{\text{K}}); E_{\text{K}} = -90 \text{ mV}; \dot{m} = (m_{\infty} - m)/\tau_m;$$

$$\dot{h} = (h_{\infty} - h)/\tau_h$$

$$m_{\infty} = 1 / (1 + \alpha_m); \alpha_m = \exp[-0.038(1.8 + 1 / \{1 + \exp[(V + 40)/5]\})(V + 1)]$$

$$\tau_m = 2 \beta_m / (1 + \alpha_m); \beta_m = \exp[-0.038(0.7 + 1 / \{1 + \exp[(V + 40)/5]\})(V + 1)]$$

$$h_{\infty} = 1 / (1 + \alpha_h); \tau_h = 0.26(V + 50); \alpha_h = \exp[0.11(V + 56)]$$

Nonspecific hyperpolarization activated cation current:

$$I_{\text{h}} = g_{\text{h}} m (V - E_{\text{h}}); E_{\text{h}} = -30 \text{ mV}; \dot{m} = (m_{\infty} - m)/\tau_m;$$

$$\tau_m = 90 \beta_m / (1 + \alpha_m)$$

$$m_{\infty} = 1 / \{1 + \exp[(V + 81)/8]\}; \alpha_m = \exp[0.08316(V + 75)];$$

$$\beta_m = \exp[0.033264(V + 75)]$$

Slow, noninactivating, potassium current:

$$I_{\text{Km}} = g_{\text{Km}} m (V - E_{\text{K}}); E_{\text{K}} = -90 \text{ mV}; \dot{m} = (m_{\infty} - m)/\tau_m$$

$$\tau_m = 1 / (\alpha_m + \beta_m); \alpha_m = 0.001(V + 30) / \{1 - \exp[-(V + 30)/9]\}$$

$$m_{\infty} = \alpha_m / (\alpha_m + \beta_m); \beta_m = -0.001(V + 30) / \{1 - \exp[(V + 30)/9]\}$$

High-voltage activated L-type calcium current:

$$I_{\text{Ca}}^{\text{HVA}} = g_{\text{Ca}} m^2 h (V - E_{\text{Ca}}); E_{\text{Ca}} = 140 \text{ mV}; \dot{m} = (m_{\infty} - m)/\tau_m;$$

$$\dot{h} = (h_{\infty} - h)/\tau_h$$

$$m_{\infty} = \alpha_m / (\alpha_m + \beta_m); \alpha_m = -0.055(V + 27) / \{\exp[-(V + 27)/3.8] - 1\}$$

$$\tau_m = 1 / (\alpha_m + \beta_m); \beta_m = 0.94 \exp[-(V + 75)/17]$$

$$h_{\infty} = \alpha_h / (\alpha_h + \beta_h); \alpha_h = 0.000457 \exp[-(V + 13)/50]$$

$$\tau_h = 1 / (\alpha_h + \beta_h); \beta_h = 0.0065 / \{\exp[-(V + 15)/28] + 1\}$$

R-type calcium current:

$$I_{Ca}^R = g_{Ca} m^3 h (V - E_{Ca}); E_{Ca} = 140 \text{ mV}; \dot{m} = (m_{\infty} - m) / \tau_m;$$

$$\dot{h} = (h_{\infty} - h) / \tau_h$$

$$\tau_m = 50 \text{ ms}; m_{\infty} = 1 / \{1 + \exp[-(V + 44)/3]\}$$

$$\tau_h = 5 \text{ ms}; h_{\infty} = 1 / \{1 + \exp[(V + 49)/1]\}$$

Slow afterhyperpolarizing potassium current:

$$I_{sAHP} = g_{sAHP} m^3 (V - E_K); E_K = -90 \text{ mV}; \dot{m} = (m_{\infty} - m) / \tau_m$$

$$m_{\infty} = [Ca^{2+}]^2 / ([Ca^{2+}]^2 + 0.025^2); \tau_m = 0.025^2 / (0.03 [Ca^{2+}]^2 + 0.025^2)$$

## RESULTS

### Synaptic transmitter release model

The reconstructed dendritic tree of a CA1 pyramidal neuron was used for all of the simulations presented here (see METHODS). The compartmental model of the dendritic tree included active currents governed by Hodgkin-Huxley kinetics. Excitatory synapses were located on the apical dendritic branches. There were no inhibitory synapses (Fig. 2A).

One of the main goals was to study the impact of presynaptic short-term plasticity on the properties of postsynaptic neuronal firing patterns. A visual inspection of Fig. 2B suggests that, when subjected to random uncorrelated series of APs, model synapses responded with complex, irregular, patterns of successful vesicle releases. To further characterize the transformation of different signals by presynaptic plasticity, we probed model synaptic responses to AP series of increasing randomness (but all delivered at the same mean rate). As is shown in Fig. 2C1, synaptic plasticity increased the variability of release events, with higher rate inputs to the synapses leading to more irregular response. Induction of variability in synaptic responses did not significantly depend on the level of calcium flux into the synapse (Fig. 2C2) but showed strong dependence on the value of the replenishment time  $\Delta T_R$  (Fig. 2C3), suggesting that depression is a dominant factor in the generation of highly variable synaptic responses.

Next, we used rhythmic stimulation patterns and matched the responses of our model to experimental measurements at CA3–CA1 hippocampal synapses (Dobrunz and Stevens 1997). The stimulus used here was a 10-Hz train of 20 regularly spaced stimuli, repeated over 100 model synapses. Figure 2, D1 and D2, shows that, depending on the values of synaptic parameters (such as the maximal number of vesicles in readily releasable pool and/or magnitude of calcium influx into the synapse), the model synapses exhibited facilitation followed by depression. The response typically became strongest after three to five stimuli, in agreement with Fig. 4C of Dobrunz and Stevens (1997). Halving the ISI did not significantly change the facilitating part of the response but led to a quicker onset of depression (Fig. 2D5).

The response also depended on the rates of calcium unbinding from the synaptic gate. For example, setting all of the unbinding rates to be equal to the slowest one (i.e., to  $k_1^-$ )

resulted in a strong response to the first stimulus (Fig. 2D3) and a significant level of asynchronous release (data not shown) that acted to quickly deplete the vesicular pool and virtually block all responses to subsequent stimuli. Setting all of the unbinding rates to be equal to the fastest one (i.e., to  $k_4^-$ ) resulted in no facilitation and very low (close to 0) probability of release (data not shown) because the probability of having fully occupied gate sites was small. Consistent with this, when the unbinding rates were set to the second fastest rate (i.e., to  $k_3^-$ ), there was significant probability of release for most of the stimuli (Fig. 2D3).

To test the effect of the RRP replenishment time on model synaptic response, we performed simulations of the model with stochastic replenishment of RRP (in a model with fixed replenishment time, the response to a rhythmic stimulation yielded the same results as long as the stimulation period was smaller than the fixed replenishment time,  $\Delta T_R$ ; Fig. 2D4). In general, increasing the replenishment time decreased the probability of observing synaptic vesicle release in response to stimulation.

Finally, we tested how the paired-pulse ratio (PPR) in our model depends on the characteristics of synaptic terminal. A change in the synaptic calcium signal (while keeping the number of vesicles fixed) led to a change in the PPR but had nearly no effect on its trial-to-trial variability (Fig. 2, E1 and E2). In contrast, the same kind of manipulation but with a larger number of vesicles per synapse led to a change in the PPR and also affected its trial-to-trial variability (Fig. 2, E3 and E4).

### Processing of synaptic signal by CA1 pyramidal neurons depends on the extent of synaptic depression/facilitation

Previous studies of synaptic integration driven by a large number of synaptic inputs have assumed that the statistics of synaptic release events followed the statistics of presynaptic spikes, which are often modeled as a Poisson process (Li and Ascoli 2006). However, presynaptic short-term plasticity affects input-output properties in a way that cannot be captured with simple Poisson-like spike trains; indeed, in our model, uncorrelated Poisson input spike trains were transformed into highly correlated sequences of successful releases (Fig. 2C). How are these temporally correlated release patterns processed by the dendritic trees in CA1 pyramidal neurons? To gain insight, we analyzed the responses of the model CA1 pyramidal neuron subject to input stimuli transformed by the model synapses.

The membrane potential in the dendritic compartments was highly irregular as was the output spike train in the soma (Fig. 3A). The firing rate of the neuron, shown in Fig. 3B, increased with the input firing rate, in accordance with previous studies (Li and Ascoli 2006). However, the output spike time series had unusually high variability (Fig. 3C). The degree of output variability depended on the presynaptic depression. At a given input rate, the variability measure  $CV_2$  (see METHODS for definition) of output spike time series of model pyramidal neuron was highest for short-term synaptic depression with a long recovery time (high  $Ca^{2+}$  influx) and lower for shorter recovery times (Fig. 3C).

The effect of depression depended on the input frequency. When plotted versus output rate, the output variability tended to be smaller at lower output (input) rates than for higher output (input) rates, as shown for the high  $Ca^{2+}$  influx case (circles) in Fig. 3C. This was unexpected, given that in cortical

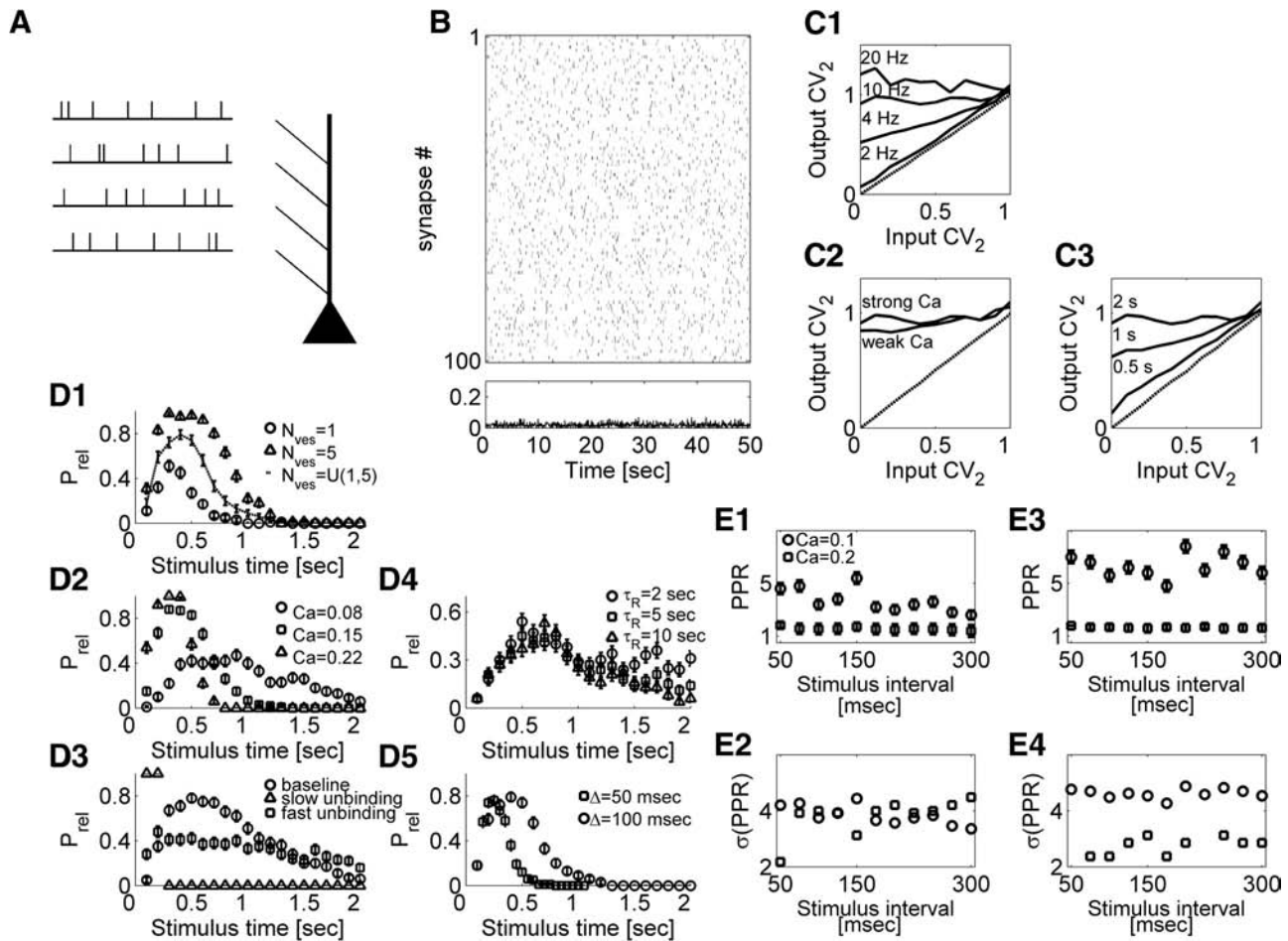


FIG. 2. Model for synaptic transmission. *A*: schematic modeling paradigm: uncorrelated Poisson input spike trains, transformed by a model of short-term presynaptic plasticity, activate fast excitatory currents at synapses on the dendrites of a multicompartamental model of a CA1 pyramidal neuron. *B*: *top*: rastergram showing a series of successful quantal releases for 100 model synapses that were stimulated by uncorrelated Poisson spike trains at an input rate  $v_{in} = 2$  Hz. *Bottom*: synaptic activity histogram (fraction of synapses releasing in the same temporal bin). *C*: transfer properties of the model for stochastic synaptic response. In all plots, dashed lines represent the response of a deterministic synapse. *C1*: when stimulated with spike trains of different variability (from completely regular to pure Poisson), model synapses generated stochastic responses that could be captured by relatively high values of variability measure,  $CV_2$ , applied to the series of inter-release intervals. The extent of variability in inter-release intervals depended on the input frequency, with higher-rate inputs causing more variable synaptic responses at all levels of input irregularity. *C2*: the variability of synaptic inter-release series only weakly depended on the level of calcium flux into model synaptic terminals. *C3*: variability could be controlled by changing the value of recovery time  $\Delta T_R$  (labeled on curve) from synaptic depression. Data points in all plots are averages over 50 model synapses. *D*: model synaptic responses to rhythmic stimulation. Periodic trains of 20 stimuli at 10 Hz were applied as in Dobrunz and Stevens (1997). The shape of the response curve could be controlled by changing the number of vesicles per model synaptic terminal (as shown in *D1* for fixed calcium signal,  $Ca^{2+} = 0.2$ ), by changing the strength of synaptic calcium signal (as shown in *D2* for fixed number of vesicles per synaptic terminal,  $N_{ves} = 3$ ), by changing the rates of calcium ion unbinding from the sensor (as shown in *D3* for  $N_{ves} = 3$ ,  $Ca^{2+} = 0.1$ ), or by changing the recovery time from synaptic depression (as shown in *D4* for  $N_{ves} = 3$ ,  $Ca^{2+} = 0.1$ , and stochastic recovery model of synaptic transmission). *D5*: decrease in the interstimulus interval from 100 to 50 ms led to faster onset of depression, which only weakly affected timing of the peak synaptic response. All values are averages and their SE. *E*: characteristics of paired-pulse ratio, defined as a change in response to a 2nd stimulus relative to the 1st plotted vs. the interstimulus interval (ISI) for different manipulations of synaptic parameters. *E1*: averaged paired-pulse ratio and SE. Circles,  $N_{ves} = 3$ ,  $Ca^{2+} = 0.1$ ; squares,  $N_{ves} = 3$ ,  $Ca^{2+} = 0.2$ . *E2*: trial-to-trial variability of paired-pulse ratios shown in *E1*. *E3*: averaged paired-pulse ratio and SE. Circles,  $N_{ves} = 3$ ,  $Ca^{2+} = 0.1$ ; squares,  $N_{ves} = 3$ ,  $Ca^{2+} = 0.2$ . *E4*: trial-to-trial variability of paired-pulse ratios shown in *E3*.

neurons (Softky and Koch 1993) as well as in simple one-dimensional integrate-and-fire models (Troyer and Miller 1997), the variability of spiking goes down with increasing output rate. In contrast, the output variability for a neuron having synapses with much faster recovery time (squares) decreased with increasing input rates.

Next, we wanted to assess the effect of facilitation on the firing rate and variability of our model pyramidal neuron. Facilitation (changes in vesicle release probability caused by enhanced binding of calcium to sensors) in our model depended on the strength of presynaptic calcium signal (Fig. 2*D2*). As Fig. 3*C* shows, strong variations in the magnitude of

the presynaptic  $Ca^{2+}$  signal had relatively small effect on the irregularity of neuronal spike trains. However, reduction of release probability (by lowering  $Ca^{2+}$  flux) led to a decrease in the output rate (Fig. 3*B*).

Softky and Koch (1993) pointed out that nonstationarity introduced by spike frequency adaptation may distort the results of variability analysis. To check the general validity of our conclusions regarding the variability of spiking, we separated the data set for each simulation scenario into two subsets of fast (<200 ms) ISIs and slow (>200 ms) ISIs. Figure 3*D* shows CVs for fast/slow subsets of ISI series, plotted for different simulation scenarios and different input rates (scat-

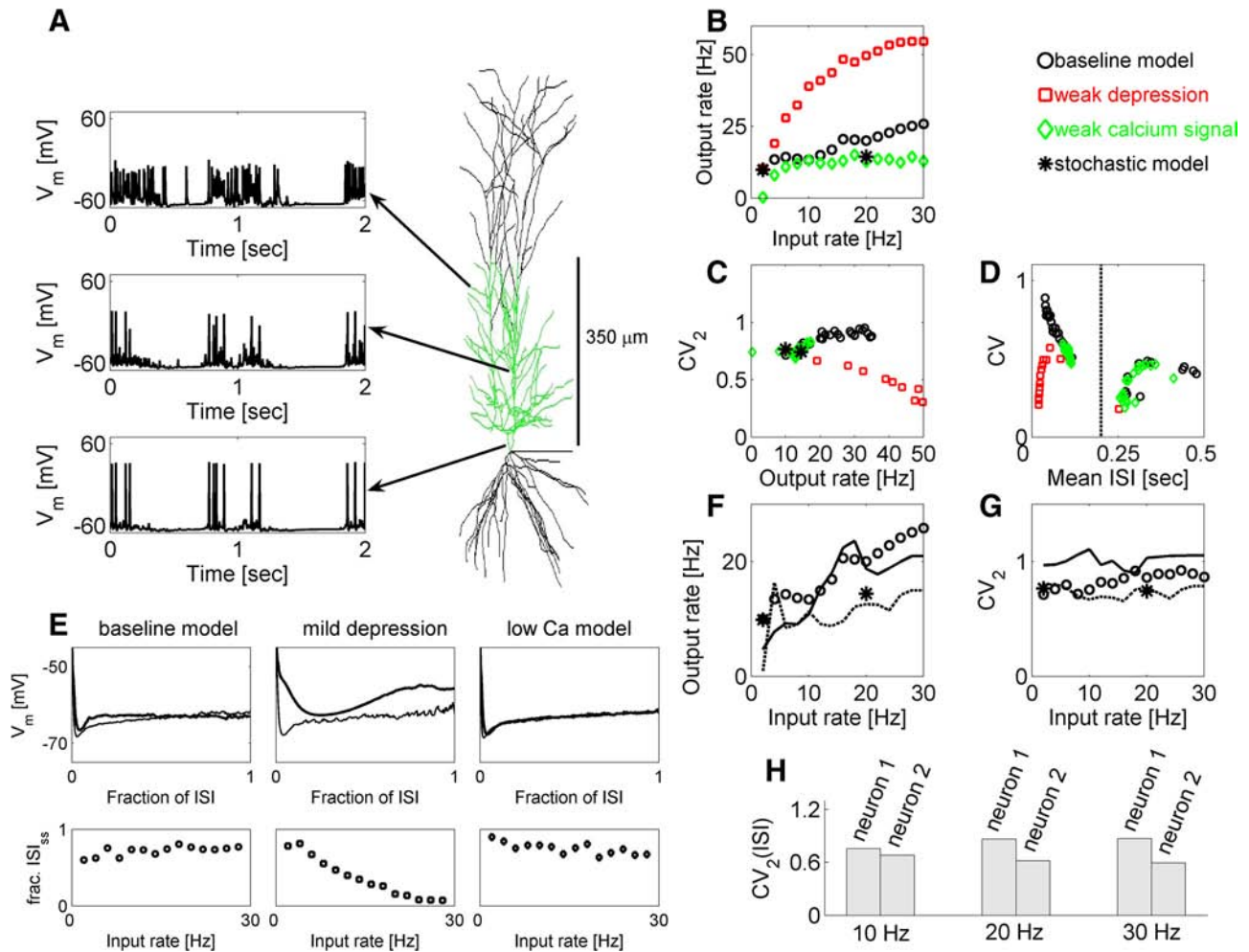


FIG. 3. Presynaptic plasticity modulates the rate and the variability of firing in a model of a CA1 pyramidal neuron. *A*: membrane potential in different compartments of a model pyramidal neuron firing in response to Schaffer collaterals stimulation. *Top*: secondary branch of apical dendrite (300  $\mu\text{m}$  away from soma). *Middle*: main trunk of apical dendrite (100  $\mu\text{m}$  away from soma). *Bottom*: somatic compartment. Synaptic inputs were uniformly distributed over the 1st 350  $\mu\text{m}$  from soma (green region of the reconstructed dendritic tree). *B*: firing rate of a model neuron as a function of input rate of spikes arriving at model presynaptic terminals: Baseline model with high presynaptic  $\text{Ca}^{2+}$  influx and long recovery time from depression (black circles); model with lower presynaptic  $\text{Ca}^{2+}$  influx (green diamonds); and model with weaker synaptic depression, as captured by shorter recovery time (red squares). Stars are for the model with stochastic recovery from synaptic depression. *C*: firing variability measure,  $\text{CV}_2$ , as a function of output firing rate, for the 3 scenarios shown in *B*. *D*: CV of interspike interval series plotted vs. the mean ISI, for different scenarios in which ISIs were partitioned into 2 groups of short and long intervals. Scatter points are for different frequencies of synaptic stimulation. Symbols are the same as for *B*. *E*: *top*: mean postspike somatic membrane voltage plotted vs. the fraction of ISI traversed for different scenarios of synaptic plasticity. In all plots, thin black traces are for 2-Hz synaptic stimulation, and thick black traces are for synaptic stimulation at 20 Hz. *Bottom*: fraction of ISI in the steady-state regimen plotted vs. the stimulation rate of model synapses for each of the model scenarios shown in the *top panels*. *F*: output firing rate plotted vs. input rate for a model in which all synaptic calcium binding/unbinding rates were equalized to the slowest value (solid line) or the fastest value (dashed line). Circles show the results obtained for the baseline model, with heterogeneous binding/unbinding rates. Stars are for the model with stochastic recovery from synaptic depression. *G*: variability measure plotted vs. input rate for all conditions shown in *F*. *H*: variability measure of ISI for the pyramidal neuron model used in the rest of this study (*neuron 1*) compared with the variability measure for another reconstructed pyramidal neuron (*neuron 2*) obtained for the same level of synaptic stimulation.

ter). As can be seen, the baseline model (circles) and the model with low calcium signal (diamonds) exhibited much stronger variability for both fast and slow ISIs than did the model with mild depression (squares). Also note that for the short ISI subset, the degree of variability exhibited by both baseline and “low calcium” models was an increasing function of output rate, whereas in the case of the model with mild depression the variability decreased for higher output rates. This analysis suggests that high variability of firing that is observed in our model neurons is a generic feature rather than an artifact that could arise because of the specific methods of analysis.

To assess the robustness of the high variability of neuronal spike time series in the presence of large number of

synaptic inputs with respect to the detailed neuronal morphology, we simulated another reconstructed pyramidal neuron (cell geo5038804, available for download from [www.neuromorpho.org](http://www.neuromorpho.org)). The simulations shown in Fig. 3*H* confirm that the variability of spike time series was not a consequence of the specific details of a single pyramidal neuron. The variability of the postsynaptic firing patterns in both morphologies depended on the short-term presynaptic depression.

Finally, we performed another test to probe the effect of vesicle release facilitation on the firing rate and variability in our model neuron. Because facilitation in our model synapses depended on the rate of synaptic calcium unbinding, we re-

soned that a change in unbinding rates might provide us with hints to how facilitation impacts variability. We performed two tests. In the first set of simulations with strong facilitation, all calcium unbinding rates were equalized to the slowest one, whereas in a second set of simulations, with weak or no facilitation, we equalized all the unbinding rates to the fastest one among the four rates shown in Table 1. Results of these simulations are summarized in Fig. 3, *F* and *G*. Setting all unbinding rates to either slow (solid line) or fast (dashed line) values decreased the output firing rate. However, variability of spiking was affected differently by the different manipulations on gating: for a model with all slow rates, the  $CV_2$  measure attained slightly higher values than for a model with all fast rates.

Troyer and Miller (1997) developed a simple framework to explain spike time series variability in cortical neurons. According to this framework, the dynamics of membrane voltage during an ISI can be divided into three qualitatively different phases: the initial refractory phase in which the neuron is recovering from the previous spike and firing is completely described using arguments based on  $1/\sqrt{N_s}$ ; the final steady-state regimen in which the “memory” about the last spike has decayed and in which spike generation is determined solely by input statistics; and the intermediate phase of partial recovery from postspike AHP, linking between the  $1/\sqrt{N_s}$  and steady-state regimens. The variability of ISI series is determined by the relative contribution from each of these regimens (the fraction of mean ISI spent in these regimens). In particular, the variability of ISI should be higher if a larger fraction of the ISI is spent in the steady-state phase, during which the time of the next spike is determined solely by the fluctuation in synaptic input. Note also that this analysis explains the contribution of postspike AHP to spike time series variability, but variability can also be affected by the changes in input (i.e., input statistics in the steady-state phase). We applied this framework to our model.

The benchmark model neuron spent less time in postspike hyperpolarization phase with high rates of inputs than for low rates (Fig. 3*E*, *left top* and *bottom*). Therefore even though the mean ISI was larger for low-rate inputs, the fraction of the ISI in the steady-state regimen was larger for the case of neuron driven by high rate inputs (Fig. 3*E*, *left bottom*), leading to more variable spike time series. In the model with weaker depression, the fraction of ISI in the steady-state regimen significantly decreased with increasing input rate (Fig. 3*E*, *middle top* and *bottom*, cf. Fig. 3*E*, *left*). On the other hand, the reduced synaptic calcium signal increased the time to the next spike, thus reducing the firing rate, but not significantly changing the fraction of ISI in the steady-state regimen, and thus had little or no effect on the spike time series variability (Fig. 3*E*, *right top* and *bottom*). This analysis is consistent with the intuitive picture in Troyer and Miller (1997).

These observations suggest that different aspects of presynaptic short-term plasticity affect the spike train of a pyramidal neuron with active dendrites in different ways. Fast vesicular turnover increased the output firing rate and reduced the spike train variability at higher input rates. Significantly lowering the probability of transmitter release reduced the output rate, but did not significantly affect the variability of output spike train. Reducing the time of relaxation from facilitation (by setting all of the calcium unbinding rates to the fastest one) acted to lower the variability of output firing, but also acted to decrease the

firing rate. Thus the gain and irregularity depended on the relative contribution from short-term presynaptic depression (changes in RRP size and/or vesicle recovery time) and short-term facilitation ( $Ca^{2+}$ -mediated modulation of individual vesicle release probability). Because the variability could be changed by manipulations of synaptic plasticity parameters and because active dendritic conductances are known to affect neuronal input-output properties (Reyes 2001), the above results led us to investigate the contribution of these conductances to spike time series variability.

#### *Dendritic processing of synaptic plasticity depends on the balance between fast inward and outward currents*

How was it possible for our model pyramidal neuron to preserve output variability despite a large number of excitatory synaptic inputs? When all active conductances were removed from the dendritic compartments, the output spikes from the model neuron became highly regular, as shown in Fig. 4*B* (closed black circles). The output firing rate, shown in Fig. 4*A*, quickly saturated, notwithstanding the presence of presynaptic depression. In addition, simulations of a point neuron driven by nonplastic synapses yielded much lower spiking variability than did the baseline model with the dendritic tree and plastic synapses at a comparable output rate (Fig. 4, *A* and *B*, black crosses). Thus while synaptic depression helped to reduce the excitatory drive and introduced significant fluctuations into release series, in itself it was not sufficient to elicit highly variable firing, suggesting that postsynaptic dendritic mechanisms might also be involved.

Furthermore, simulations of a neuron that had only fast inward and outward conductances (excluding the  $Ca^{2+}$  and slow  $Ca^{2+}$ -activated  $K^+$  currents) in its dendritic tree yielded a significantly higher firing rate (compared with the baseline model) but also reduced the irregularity of the output spike train of the full model (Fig. 4*B*, squares). On the other hand, a complete removal of the nonspecific hyperpolarization-activated depolarizing current,  $I_h$ , from dendritic compartments only insignificantly affected the firing characteristics of a model neuron (Fig. 4, *A* and *B*, closed diamonds). This suggests that, in addition to local inhibitory control (Liu 2004), the sensitivity of a neuron to synaptic fluctuations might, at least in part, be controlled by the activation of intrinsic conductances in its dendritic branches (Wilson and Kawaguchi 1996). Because inhibition was absent in our model, the control of this input sensitivity might be achieved, for example, by varying the ratio between fast inward/outward active conductances. Indeed, halving the magnitude of the A-type  $K^+$  conductance increased the output firing rate and acted to decrease the spike time series variability of the model CA1 neuron (Fig. 4, *A* and *B*, green diamonds). More generally, the rate and irregularity could be controlled by changing the expression of dendritic sodium channel conductance and A-type potassium channel conductance (Fig. 4, *C1* and *C2*). Sample traces of somatic membrane potential for these different scenarios are shown in Fig. 4*D*. Thus the capability of intrinsic conductances to modulate dendritic excitability of our pyramidal neuron could help to maintain its overall sensitivity to the plastic, activity-dependent changes in release properties of its afferent synapses.

To understand how active conductances (and in particular potassium channels) contributed to high ISI variability, we again used the mean ISI analysis of Troyer and Miller (1997). As Fig.

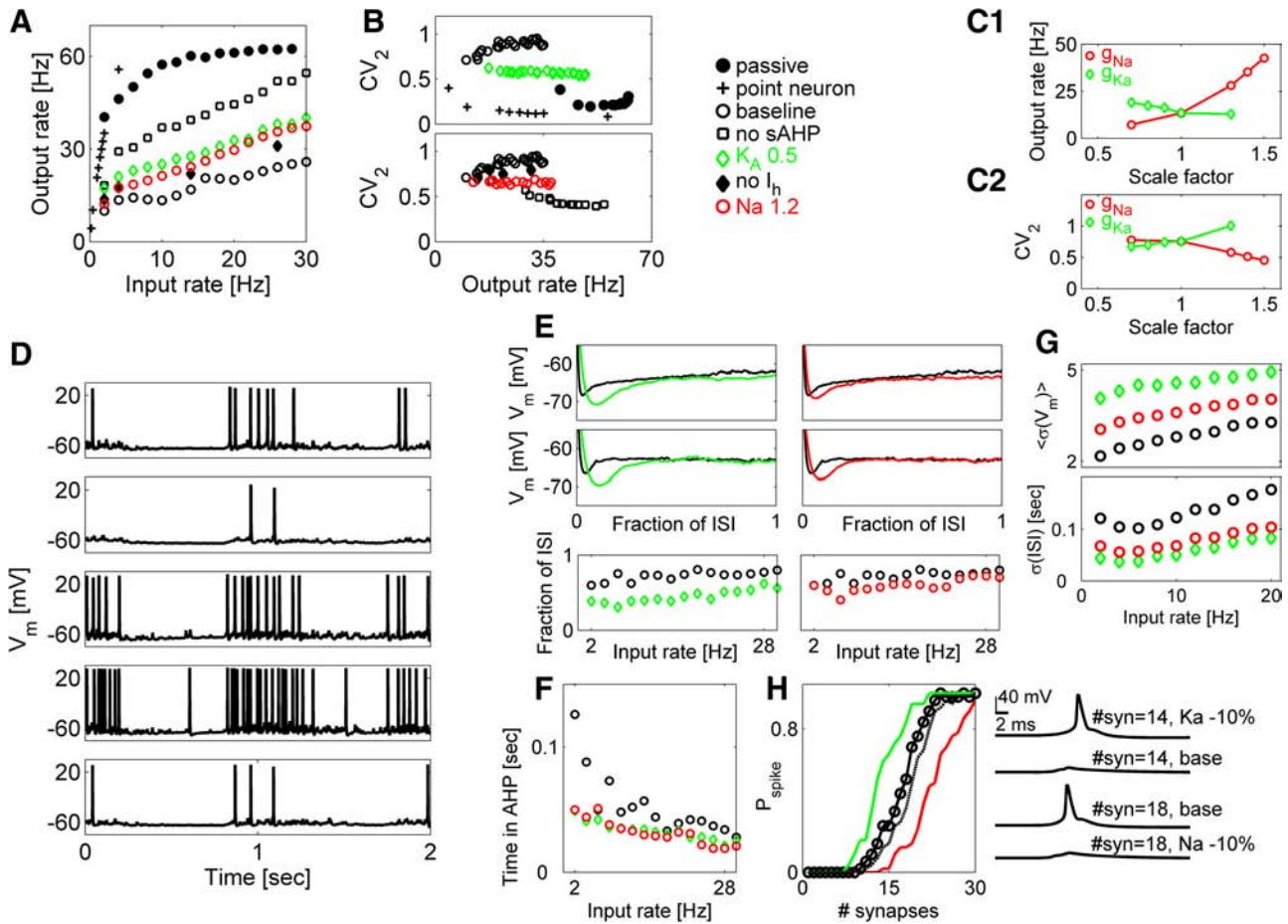


FIG. 4. Balance between inward/outward active dendritic conductances enhances output variability in response to synaptic stimulation. **A**: output firing rate as a function of input rate. Firing rate quickly saturated for a neuron with a passive dendritic tree (closed black circles) but was a less rapidly increasing function of input rate when all fast and slow conductances were present (open circles), the A-type  $K^+$  outward conductance was reduced twofold (green diamonds,  $K_a^* = 0.5K_a$ ), the dendritic Na conductance was increased by 20% (red circles), or only fast conductances (open squares) were present in the dendritic compartments. **B**: firing variability measure,  $CV_2$ , as a function of output firing rate, for all conditions shown in **A**. Note that when calcium and slow afterhyperpolarization (sAHP) conductances were removed from dendritic compartments, the variability measure attained lower values as compared with the baseline model. With the point neuron firing at the rate comparable to that of the baseline model, the variability was much lower than for the baseline model. The same keys apply to both subpanels. **C**: modulation of output firing rate (**C1**) and its variability (**C2**) by the balance between fast inward current (sodium) and fast outward current (A-type potassium). An increase in dendritic sodium channel conductance (red circles) led to an increase in firing rate and decrease in variability of spiking. Scaling of dendritic A-type potassium channel conductance (green diamonds) has exactly the opposite effect. In all cases, the stimulation frequency was 10 Hz. **D**: examples of somatic membrane potential traces for different cases analyzed in **C**. From *top to bottom*: baseline model, Na conductance scaled by 0.7, Ka conductance scaled by 0.7, Na conductance scaled by 1.3, and Ka conductance scaled by 1.3. In all cases, the stimulation frequency was 10 Hz. **E**: fractional ISI occupancy analysis for different stimulation frequencies and different scenarios of dendritic excitability. *Top left*: averaged postspike membrane potential in somatic compartment for baseline model (black trace) and  $K_a^* = 0.5K_a$  model (green trace) at 2-Hz synaptic stimulation. *Middle left*: averaged postspike membrane potential in somatic compartment for baseline model (black trace) and  $K_a^* = 0.5K_a$  model (green trace) at 20-Hz synaptic stimulation. *Bottom left*: fraction of ISI in the steady state plotted vs. the synaptic stimulation rate for baseline model (black circles) and  $K_a^* = 0.5K_a$  model (green diamonds). *Right set of panels* shows the same set of comparisons between baseline model (black traces and black circles) and the model with 20% increase in dendritic Na conductance (red traces and red circles). **F**: duration of postspike AHP plotted vs. the synaptic stimulation rate for different scenarios. Black circles, the baseline model; green diamonds, the  $K_a^* = 0.5K_a$  model; red circles, the model with 20% increase in dendritic Na conductance. **G**: *top*: averaged (over different voltage trajectories) SD of somatic membrane potential vs. the synaptic stimulation rate. Black circles, the baseline model; green diamonds, the  $K_a^* = 0.5K_a$  model; red circles, the model with 20% increase in dendritic Na conductance. *Bottom*: SD of ISI series for these 3 scenarios. **H**: probability to evoke somatic spike by synchronously activated (deterministic) synapses. Circles, the baseline model; solid red, the model in which dendritic Na channel conductance was decreased by 10% (with the level of dendritic  $K_A$  conductance fixed); solid green, the model in which dendritic  $K_A$  conductance was decreased by 10% (with the level of dendritic Na conductance fixed); dashed line, the model in which both dendritic Na and  $K_A$  conductances were reduced by 10%.

4E (3rd left panel) shows, for all input rates considered, the fraction of ISI spent in the steady-state regimen was higher for the baseline model than for the model with reduced expression of dendritic  $K_A$  conductance. This increase in fractional occupancy in the steady-state regimen could in principle be explained by a decrease in the duration of postspike AHP; however, a plot of the postspike AHP duration versus synaptic stimulation rate showed that a reduced expression of dendritic  $K_A$  conductance caused a

reduction in the duration of postspike AHP (Fig. 4F). This suggests that the dominant effect of reduced dendritic  $K_A$  conductance is to shorten the duration of the ISI (as is manifested by higher firing rate; Fig. 4A), because of the stronger fluctuation in synaptic signal that makes spike-threshold crossing more probable and regularizes the spike time series (Fig. 4G). As Fig. 4, E–G, shows, the same arguments can be applied to explain the effect of dendritic Na conductance on spike time series variability. Thus a shift

in the expression of dendritic fast inward/outward currents could affect ISI variability through a change in the probability of spike generation.

To test the validity of these observations, we assessed, for different scenarios, the probability of somatic spike generation versus the number of synchronously activated synapses. In these simulations, one stimulus was delivered to a set of reliable synapses that were randomly distributed over apical dendrites of pyramidal neuron, and somatic responses to such a stimulus were averaged over 50 independent realizations. Figure 4H shows that, in general, the probability of generating a somatic spike was a sigmoid-like function of the number of activated synapses. A 10% reduction in conductance of dendritic  $K_A$  channels (while keeping the level of Na conductance fixed) shifted the curve to the left, whereas a 10% reduction in the level of dendritic Na conductance (while keeping the level of  $K_A$  conductance fixed) produced a comparable shift to the right. In contrast, joint variation of both the Na and  $K_A$  conductances left the curve nearly unchanged.

#### *Efficient detection of slow synaptic fluctuations relies on dendritic voltage-gated calcium channels*

Removal of calcium and slow, calcium-activated AHP conductances from dendritic compartments of a neuron led to a decrease in the variability of firing (Fig. 4A, squares vs. circles). This suggested that calcium-associated mechanisms might contribute to the balance between inward and outward conductances in the model.

A change in the level of dendritic calcium channel conductance could affect the balance condition by shifting the probability to evoke somatic spike in response to synchronous stimulation of several synapses, as described in the previous section for the case of sodium and potassium channels (Fig. 4G). However, a complete removal of dendritic calcium channel conductance did not significantly affect the probability of somatic spike generation (Fig. 5C), suggesting that the fast current through dendritic calcium channels might not be the dominant factor behind spike series irregularity.

We further assessed the role of the electrical current conducted by calcium channels by examining the effect of dendritic calcium channels that increase internal calcium concentration without conducting a net current. Specifically, this was performed by adding, for each type of calcium channel, a nonspecific ionic current that was equal and opposite to the inward current conveyed by that type of calcium channel. As shown in Fig. 5, A and B (circles vs. crosses), this removal of net ionic current (without affecting the dynamics of internal calcium concentration) did not lead to any significant departure from the basic results. On the other hand, a complete removal of voltage-gated  $Ca^{2+}$  channels from dendrites dramatically increased the mean rate and reduced the variability of output spike time series. These results suggest that voltage-gated calcium channels (VGCCs) are necessary but not sufficient to explain the change in synaptic gain that occurs in the full model.

The effect of calcium channels on spike train variability might be mediated by processes activated by changes in intracellular calcium concentration rather than by the depolarizing effects of the calcium currents (Fig. 5D). Consistent with this explanation, the rate and the variability of spiking were affected by changing the characteristic time of calcium extrusion pump (Fig.

5, E and F). Thus calcium-activated sAHP, rather than the fast current through dendritic calcium channels per se, is responsible for the more variable responses that are observed in the baseline model. As is shown in Fig. 5G, activation of dendritic VGCCs after the arrival of back-propagating AP or dendritic spike led to influx of calcium that turned on slow  $Ca^{2+}$ -activated  $K^+$  conductance. This had the effect of hyperpolarizing the membrane and effectively reducing the average synaptic drive, thus shifting the balance toward the regimen of higher variability. However, the coupling of different VGCC types to slow,  $Ca^{2+}$ -activated potassium channels in dendrites is uncertain (Pineda et al. 1998; Shah and Haylett 2000), as is the precise mechanism of sAHP activation by calcium (Sah and Clements 1999).

We assessed the robustness of calcium-activated potassium channels by performing simulations with different, more detailed, models of channels underlying sAHP (METHODS). The output spike series variability was significantly higher when different sAHP channels were added to apical dendrites of the neuron (Fig. 5H). Interestingly, ISI variability was highest for the most detailed model of the sAHP that incorporated stochastic binding and unbinding of  $Ca^{2+}$  ions from sAHP channel gates (Sah and Clements 1999).

#### *Distribution and expression of dendritic sAHP affects both rate and variability gain*

Among all the active currents in dendrites, the sAHP conductance is potentially the most interesting because the rise and decay time scales ( $>100$ -ms rise,  $>1$ -s decay) are compatible to the time scales of short-term presynaptic plasticity ( $\sim 100$  ms for short-term facilitation,  $\sim 1$  s for recovery from short-term depression). Therefore the peak values of the sAHP conductance and its spatial distribution are likely to be important. Experimental evidence suggests that the sAHP  $K^+$  channels might be preferentially located in proximal apical dendrites (but see Bekkers 2000), although with uncertain density (Sah and Bekkers 1996). Therefore we first varied the peak  $\bar{g}_{sAHP}$  value in dendritic compartments, assuming the spatial profile shown in Fig. 6A. A systematic reduction of dendritic peak sAHP resulted in a rise of the firing rate (Fig. 6B) and a decrease of output variability (Fig. 6C). Interestingly, a neuron with a uniform dendritic profile of sAHP (Fig. 6A, dashed line) was still able to generate significantly variable spike time series in response to synaptic stimulation, indicating that the baseline level of sAHP might also be important. Furthermore, we assessed the importance of the specific spatial profile of dendritic sAHP conductance distribution by performing simulations for the model pyramidal neuron with altered sAHP distribution shape (Fig. 6A, gray lines; the overall dendritic sAHP conductance in this model was equal to that in the baseline model). This manipulation had little effect on the firing rate of the neuron but caused a reduction in its spike time series variability (Fig. 6, B and C, crosses). This suggests that the variability in neuronal spike time series might depend, at least in part, on the dynamics of local inward/outward conductance balance in its dendritic branches. Thus the strength and the specific distribution of dendritic sAHP defined the extent of irregularity in neuronal spike time series.

The sAHP in dendritic compartments significantly contributed to spike time series variability. In contrast, stronger somatic sAHP slightly reduced the variability (Fig. 6D, 2nd

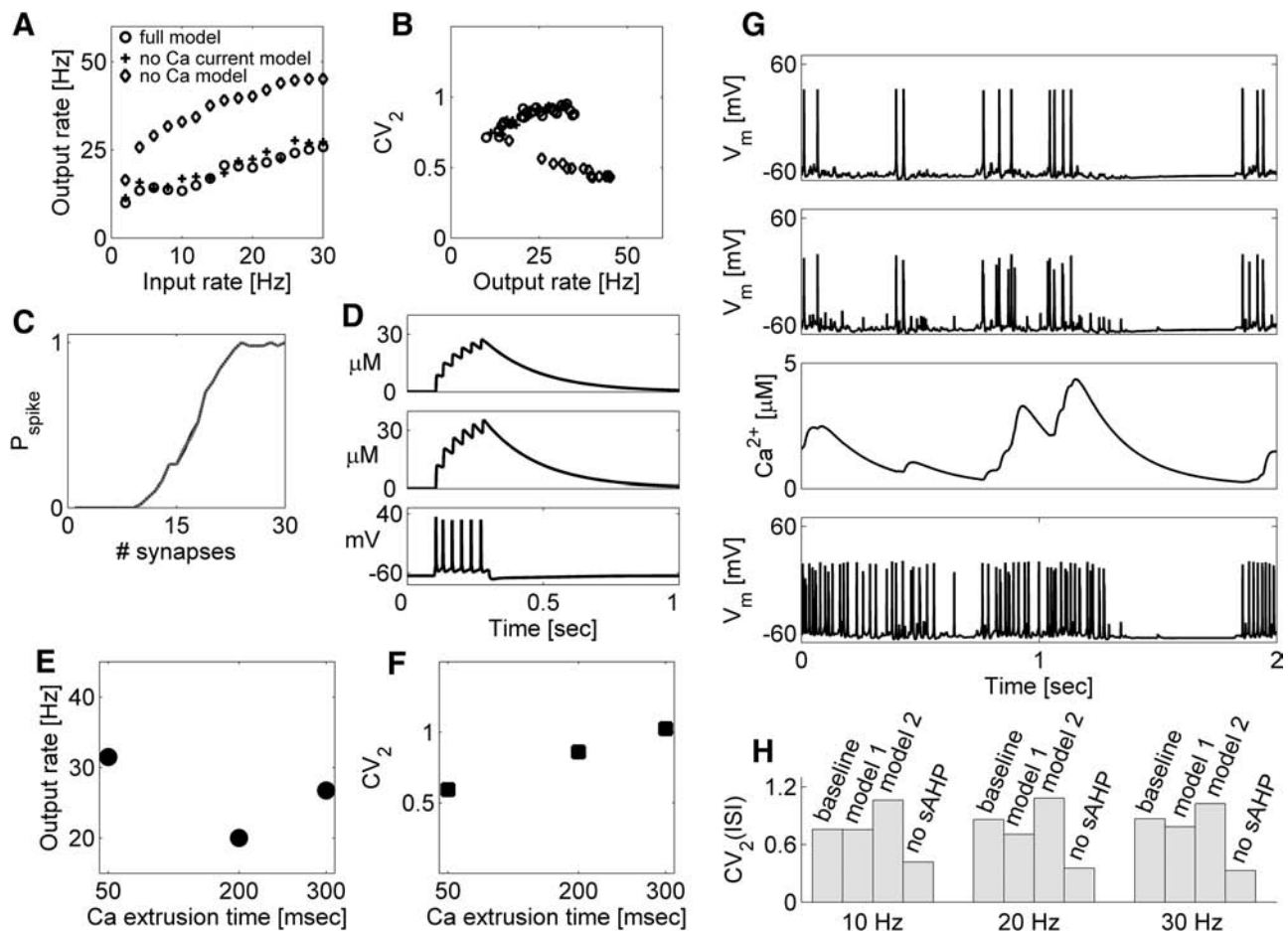


FIG. 5. Influence of voltage-gated calcium channels on the firing rate and spike variability of the CA1 pyramidal neuron. *A*: output rate as a function of input rate when all  $\text{Ca}^{2+}$  channels were removed from dendritic compartments (diamonds) compared with the baseline model in which calcium mechanisms were present in all dendritic compartments (open black circles) or with the firing rate of a neuron with altered  $\text{Ca}^{2+}$  channels that increased internal calcium concentration but did not conduct net calcium current (black crosses). *B*: firing variability measured by  $\text{CV}_2$  as a function of output rate for the conditions in *A*. *C*: probability to evoke somatic spike by synchronous activation of synapses does not depend on the level of dendritic  $\text{Ca}^{2+}$  channel conductance (the black curve for the baseline model almost coincides with the gray curve for the model without dendritic calcium channels). *D*: examples of calcium concentration build up in apical dendritic compartments in response to somatic stimulation by step current. Calcium profiles shown in the baseline model (*top*) and the model with altered calcium channel properties (*middle*). *E*: output firing rate of model pyramidal neuron plotted vs. characteristic time constant of calcium extrusion from somatic and dendritic compartments. *F*: firing rate variability, as captured by  $\text{CV}_2$ , plotted vs. characteristic time constant of calcium extrusion from somatic and dendritic compartments. Variability of spiking increased as more calcium accumulated in dendrites. *G*: typical time courses of responses. Somatic membrane potential (*top*) and the membrane potential in a dendritic compartment (*2nd panel from top*). High-amplitude fluctuations in the dendritic membrane potential led to an increased dendritic  $\text{Ca}^{2+}$  levels (*3rd panel from top*) through activation of voltage-gated calcium channels. *Bottom*: membrane potential in that same dendritic compartment as above when all dendritic  $\text{Ca}^{2+}$  channels were removed. *H*: output spike series variability for different models of sAHP plotted vs. different input stimulation rates.

panel). Analysis of the mean ISI helped to understand this difference. An increase in somatic sAHP slightly increased the mean ISI but also led to an increase in the duration of postspike refractory phase (Fig. 6*D*, 4th panel), compensating for the effect of synaptic input on variability. In comparison, an increase in dendritic level of sAHP conductance also led to an increase in the duration of postspike AHP but significantly increased the mean ISI, therefore resulting in a net increase in the fraction of ISI spent in the steady-state voltage regimen (Fig. 6*D*, 3rd panel).

How does activation of the sAHP in the model dynamically reduce the excitatory synaptic drive? One possibility is that global back-propagating APs (Fig. 1*C*) regulated local dendritic excitability by activating sAHP channels. Another possibility is that this kind of regulation is mediated by local dendritic spikes, which spread  $\sim 80 \mu\text{m}$  from their initiation

site (Fig. 1*D*). To test the latter explanation, apical dendritic branches were asynchronously stimulated by randomly distributed  $N_{\text{syn}} = 100$  deterministic synapses by 5 pulses at 20 Hz. Such stimulation generated subthreshold somatic voltage fluctuation that did not result in somatic spikes (Fig. 6*E*, *top*). A test stimulus, delivered 150 ms later by synchronous activation of  $N_{\text{sym}} = 22$  (deterministic) synapses (distributed in the earlier stimulated compartments) failed to generate somatic spike. Somatic spikes could, however, be reliably generated by the same test stimulus in the absence of any preconditioning stimulation or after the sAHP was removed from dendrites (Fig. 6*E*). These results suggest that spike-time variability could be attributed, at least in part, to the action of subthreshold synaptic stimulation and local dendritic spikes.

We further considered how different patterns of somatic spiking activity could affect subsequent neuronal firing pat-

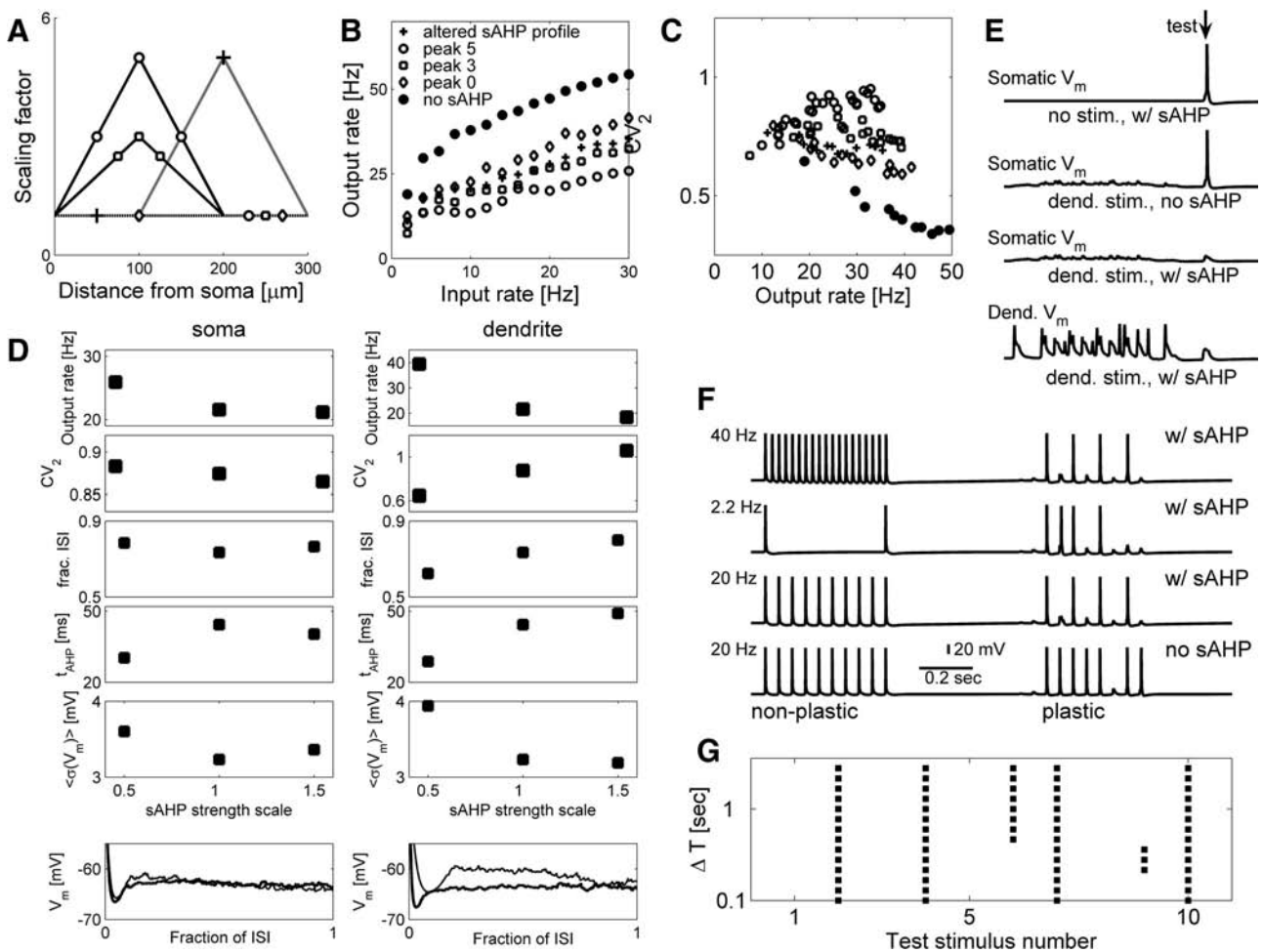


FIG. 6. Changing the distribution of dendritic sAHP conductance modulated neuronal output firing rate and firing variability. *A*: different distributions of dendritic sAHP conductances (circles, high; squares, medium; diamonds, flat) relative to that in somatic compartment ( $1 \text{ pS}/\mu\text{m}^2$ ). Solid gray line with black crosses: altered spatial profile of dendritic sAHP distribution. *B*: output firing rate as a function of input rate for different distributions shown in *A* and compared with removal of the sAHP from dendritic compartments (black closed circles). *C*: firing variability measured by  $CV_2$  vs. output rate for different distributions in *B*. *D*: *top*: firing rates obtained at 20-Hz stimulation vs. the level of somatic sAHP with dendritic sAHP fixed (*left*) and vs. the level of dendritic sAHP with somatic sAHP fixed (*right*). *Second panel*: firing rate variability for the 2 scenarios shown in the *top panel*. *Third panel*: fraction of ISI in the steady state. *Fourth panel*: duration of postspike AHP. *Fifth panel*: averaged (over different voltage trajectories) SD of postspike somatic membrane potential. *Sixth panel*: mean postspike somatic membrane potentials for low (scale factor, 0.5; thin black trace) and high (scale factor, 1.5; thick black trace) levels of somatic sAHP (*left*) and for low (scale factor, 0.5; thin black trace) and high (scale factor, 1.5; thick black trace) levels of dendritic sAHP (*right*). *E*: spike conditioning of apical dendritic branches by sub-threshold synaptic stimulation and dendritic sAHP. *F* and *G*: neuronal response to stochastic synaptic stimulation depends on the pattern (*F*) and timing (*G*) of its prior spiking activity. In *G*, the black squares in the spike raster plot mark the occurrence of spikes in response to 1 of 10 test stimuli (stimulation rate, 20 Hz) for different time intervals  $\Delta T$  from cessation of preconditioning deterministic stimulation (10 pulses at 20 Hz) to the onset of test stimulation of plastic synapses (10 pulses at 20 Hz).

terns through interaction of sAHP with fluctuating synaptic input. As shown in Fig. 6*F*, high-frequency stimulation of a neuron with deterministic synapses elicited variable responses to test stimulation with stochastic synapses ( $N_{\text{syn}} = 80$ , 10 pulses at 20 Hz), delivered after 400 ms. This variable response was a direct outcome of dendritic sAHP activation, because a removal of  $\text{Ca}^{2+}$ -dependent potassium channels resulted in a more regular response to test stimulation (Fig. 6*F*, *bottom*). Low-frequency stimulation with deterministic synapses had almost no effect on responses to subsequent test stimulus (Fig. 6*F*, *middle*). We further assessed the time scale associated with the effect of dendritic sAHP on spiking irregularity in our model by changing the interval  $\Delta T$  from cessation of preconditioning deterministic stimulation to the onset of test stimuli (as in Fig. 6*F*, *3rd panel*) and monitoring the spike responses. The spike raster plot, shown in Fig. 6*G* suggests that the effects

of dendritic sAHP persisted for  $\sim 800$  ms. Thus the effect of the dendritic sAHP on spike time irregularity depended on the characteristics of earlier neuronal spiking activity.

#### Spike number variability during theta oscillations

The principal neurons in the hippocampal formation are modulated by theta (4–8 Hz) rhythms (Buzsaki 2002). The interaction of voltage variations (caused by theta oscillation) with the various active conductances can, in principle, affect the properties of neuronal spike trains. Experimental evidence indicates that the number of spikes fired during a theta cycle is highly variable, but the origin of this variability remains unknown. To gain insight into the effects of theta rhythms on spike train variability, we injected an oscillating current into the soma of the model neuron, simultaneously stimulating the

afferent synapses with Poisson spike trains. Interestingly, the theta-like signal modulated the firing rate but did not significantly affect the variability of neuronal spike trains (Fig. 7A). The spike count (defined as a number of spikes in 1 cycle) fluctuated, with the model neuron firing between zero and four APs during one theta oscillation (Fig. 7B).

To quantify the variability in spike count, we computed the Fano factor, defined as  $FF = Var(SC)/(SC)$ , where  $SC$  is the set of spike counts. The relatively high values of the Fano factor (Fig. 7D) and the variability measure of the ISI series,  $CV_2$  (Fig. 7C), indicate that, even though the theta-modulated neuron discharged primarily during high phase of theta cycle, its firing pattern was still highly irregular. These observations suggest the variable neuronal discharge that is induced by presynaptic short-term plasticity and active dendritic branches might contribute to the variability in output of hippocampal neurons during theta activity.

The dependence of neuronal firing pattern on the previous history of stimulation is modulated by intrinsic conductances. Consider the case of a pyramidal neuron driven by two sets of plastic synapses (Fig. 7E). The synapses belonging to one set ( $N_{sym} = 80$ ) are synchronously activated, and the two sets are alternatively activated (each stimulated at 10 Hz), generating an overall 20-Hz rhythmic stimulation of fluctuating strength. As shown in Fig. 7E (top trace), in the baseline model, the response of a neuron to such a stimulus is irregular. Spike generation in response to synaptic set activation is determined here by the state of presynaptic terminals (context defined by earlier synaptic activity) and by the pattern of spike time series of that same neuron (context defined by active dendritic conductances and dendritic sAHP). On the other hand, when a dendritic sAHP is blocked, the sensitivity to synaptic context is greatly reduced (Fig. 7E, 2nd trace).

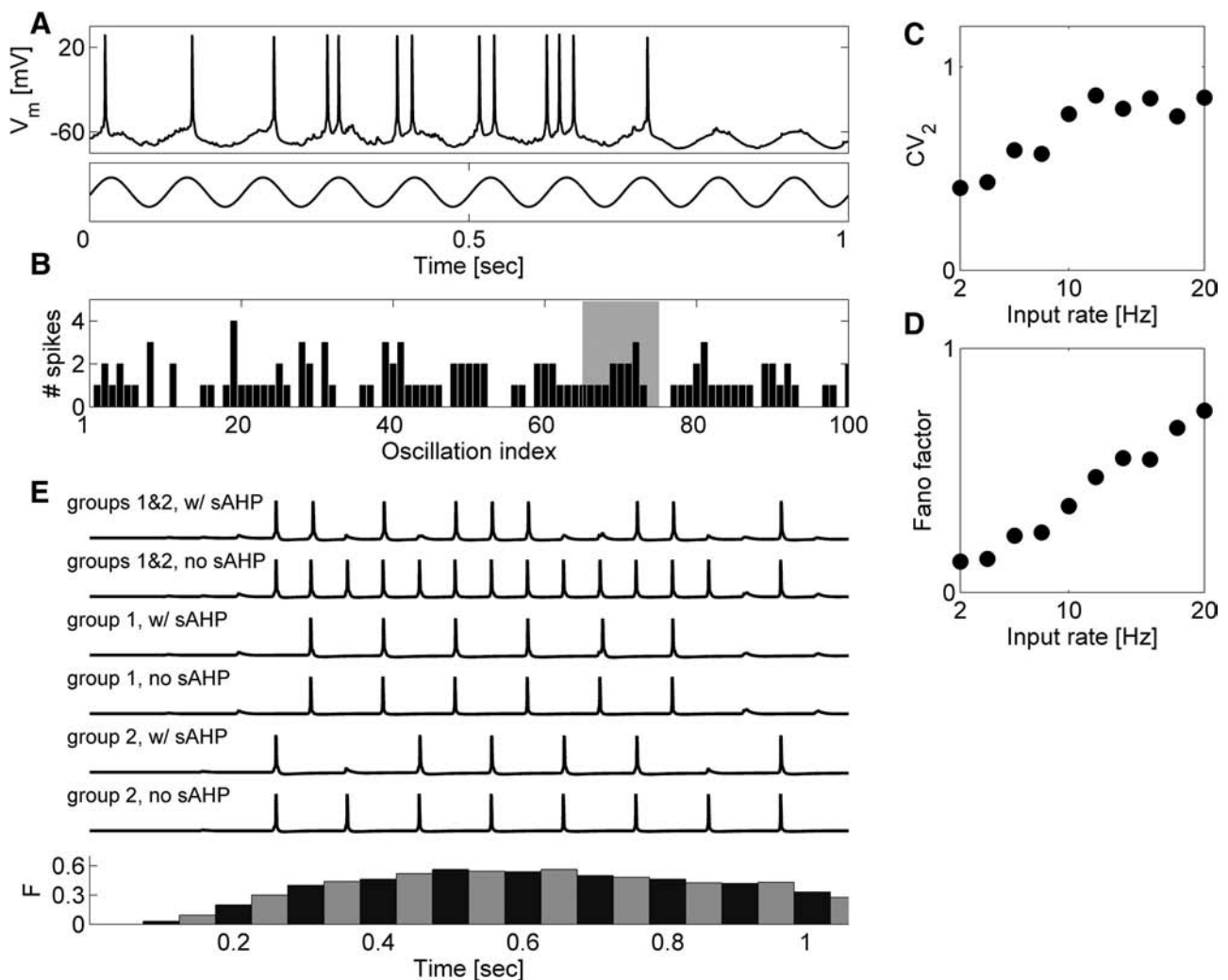


FIG. 7. Response of a synaptically activated model pyramidal neuron to somatic theta rhythm modulation. *A*: membrane potential in the somatic compartment of a neuron that was modulated by theta-like current injection and synaptically stimulated by  $v_{stim} = 20$ -Hz Poisson spike trains. A periodic current  $I(t) = 0.2 \text{ nA} \times \sin(2\pi \times f \times t)$ , with  $f = 10 \text{ Hz}$ , was injected into somatic compartment (*bottom*). *B*: spike count (number of spikes per theta oscillation) also exhibited significant variability. The shaded region corresponds to the time interval shown in *A*. *C*: output firing variability vs. input rate. *D*: the variability of output spike count, as captured by Fano factor, as a function of input rate. *E*: context-dependent response to synaptic stimulation. Top trace: Somatic membrane potential of pyramidal model neuron in response to rhythmic and alternating stimulation by 2 sets of synapses. Second trace: somatic membrane potential of pyramidal model neuron driven by the same pattern of stimulation, but with sAHP removed from apical dendrites. Third to Sixth traces: somatic membrane potential of pyramidal model neuron when only 1 of synaptic groups is activated, with and without sAHP in apical dendrites of a model neuron. Bottom histogram: fraction,  $F$ , of synapses (gray and black represent 2 different sets of synapses) that release during the train of stimuli corresponding to the top trace.

## DISCUSSION

The sensitivity of a neuron to correlated synaptic inputs depends on balancing the overall excitatory and inhibitory synaptic inputs to a neuron (Salinas and Sejnowski 2000). We showed here that balancing with inhibitory inputs is not necessary for this to occur. Using a biophysically realistic model of use-dependent short-term presynaptic plasticity at excitatory synapses and active dendritic conductances, we showed that a balance of inward and outward currents within dendritic compartments yields a high degree of variability in the output spike train. This depended in part on the slow potassium current (sAHP), which matched the slow time scale synaptic fluctuations arising from presynaptic short-term plasticity. Previously, fast outward dendritic currents were suggested as a possible way to maintain output variability (Prescott and Sejnowski 2008; Softky 1995), without considering presynaptic mechanisms.

Dendritic potassium conductances counteracted strong excitatory drive that would otherwise decrease the irregularity. This is consistent with an earlier study of spiny neostriatal neurons, in which potassium channel activation governed the transition of the membrane voltage from up to down states, counteracting strong synaptic excitation (Wilson and Kawaguchi 1996). We also showed that potassium channels, and in particular calcium-activated potassium channels, can maintain high output irregularity when dendrites are driven by many synapses with short-term plasticity. This depended on the dendritic balance between fast inward and outward currents, which allowed the fluctuating synaptic signals to generate somatic spikes, as well as the dendritic calcium-activated potassium channels, which adjusted the excitability of dendritic branches to the global and local spiking activity. These results suggest that dendritic potassium channels can to some extent replace synaptic inhibition in balancing synaptic excitation and endowing the neuron with an additional, autonomous way to regulate spiking.

Although fast active conductances were able to support some dendritic variability, the inclusion of relatively slow channels, such as the  $\text{Ca}^{2+}$ -activated slow  $\text{K}^+$  currents, enhanced the sensitivity of the dendrites to the slow, activity-dependent fluctuations in the synaptic inputs. In our model, dendritic sAHP could be activated either by back-propagating APs or by local dendritic spikes that spread to a limited distance ( $\sim 80 \mu\text{m}$ ) from the site of their initiation (Fig. 1D). Taken together with the strong independence of pyramidal neurons dendritic branches (Poirazi et al. 2003b) and spatially nonuniform distribution of sAHP, this leads to the notion of “local balance,” in which the branch-specific distribution of dendritic conductances, and in particular of sAHP, defines the sensitivity of that branch to patterns of synaptic stimulation. Although the precise definition of locality depends on many factors (such as, for example, the spatial distribution of synaptic terminals on apical dendrites or the precise distribution and variety of active conductances), we postulate that the range of dendritic spike propagation ( $80\text{--}100 \mu\text{m}$ ) or branch length is the relevant spatial scale.

The primary effect of sAHP is to increase membrane conductance and therefore change the membrane mode from integration to coincidence detection (Andreasen and Lambert 1995; Softky and Koch 1993). It is reasonable to assume that,

under physiological conditions, the transients in dendritic calcium are compartmentalized by dendritic spines and rarely spread by diffusion through the entire tree (Andreasen and Lambert 1995; Yuste and Denk 1995). In this situation, dendritic membrane conductance at a given synaptic site could fluctuate depending on the expression of sAHP conductance in the immediate proximity ( $\sim 4 \mu\text{m}$ ) of that synapse and on the ongoing collective synaptic activity within  $\sim 80 \mu\text{m}$  from that synapse, thus reinforcing the activity-dependent fluctuation in synaptic drive and leading to variable neuronal discharge (Schwindt and Crill 1997). This raises the interesting question of whether the expression of sAHP channels in dendrites is directly controlled by the distribution and activity of synapses (Stemmler and Koch 1999). Interestingly, several recent studies suggest that the regulation of sAHP might control the heterosynaptic induction of long-term potentiation and long-term depression in CA1 pyramidal cells (Le Ray et al. 2004). Taken together with our findings, these observations call for a detailed study of the contribution of the sAHP to long-term synaptic plasticity.

Different sites of synaptic input can “communicate” through back-propagating APs and/or dendritic spikes, as occurred in the model. Significantly, even without these two mechanisms, sufficient depolarization of the postsynaptic membrane resulting from intense synaptic stimulation can allow large influx of  $\text{Ca}^{2+}$  through NMDA- and voltage-gated calcium channels (Magee et al. 1995), with possible subsequent diffusion of  $\text{Ca}^{2+}$  signal and activation of calcium-dependent  $\text{K}^+$  channels at nearby nonactive synapses. For this to happen, however, synaptic sites would have to be sufficiently clustered, and their activity would have to be sufficiently intense and correlated in time, to generate a  $\text{Ca}^{2+}$  signal strong enough to diffuse for a significant distance along the dendritic tree (Larkum and Nevian 2008). Because the afferents in our model were uniformly distributed along the dendrites and were activated at random times, and strong presynaptic depression significantly reduced the excitatory drive at individual synapses, the effects of  $\text{Ca}^{2+}$  diffusion and buffering were negligible, and the probability of activating the sAHP conductance by coordinated action of spatially proximal synapses was small. However, exactly how complex patterns of synaptic organization and activity might affect the integrative properties of pyramidal neurons through diffusion-mediated long-range calcium signaling is a question that should be further explored (Gasparini and Magee 2006; Larkum and Nevian 2008).

In a recent study of synaptic integration in CA1 dendritic trees (Gasparini and Magee 2006), asynchronous inputs randomly distributed as in our model produced approximately linear summation in the dendritic branches; however, when synaptic inputs arrived synchronously and were spatially clustered in a single dendritic compartment, the clustered input produced a highly nonlinear integration that led to an AP at the soma that was remarkably precise and invariant. This suggests that these neurons have two modes for integrating dendritic inputs that favors rate processing for randomly arriving inputs and temporal processing for synchronously arriving inputs. The dendritic balance obtained by the mechanisms studied here could explain the observed sensitivity of dendritic branches to correlated synaptic inputs.

This study focused on the effect of excitatory inputs from Schaffer collaterals and did not include the contribution of

feedback and feed-forward inhibition on the activity of CA1 neurons. Reproducing the effects of inhibition in a single neuron model is quite challenging, because feed-forward inhibition from CA1 interneurons is activated by inputs from CA3 region, and the exact interconnectivity pattern of these interneurons is largely unknown. Nevertheless, recent experimental evidence has indicated that there is a local dendritic structural and functional balance between excitation and inhibition (Liu 2004) and that excitatory and inhibitory synapses on CA1 pyramidal cells act in synergy to enhance synaptic gain in these neurons (Klyachko and Stevens 2006). There is also strong inhibition on the soma, in addition to inhibitory modulation of local excitability in individual dendritic branches. These inhibitory effects enhance the ability of a neuron to detect synaptic fluctuations and could act synergistically, at different time scales, with the mechanism of dendritic balance by sAHP suggested here.

CA1 pyramidal neurons in the hippocampus respond selectively to locations in an environment (O'Keefe and Nadel 1978). In experiments performed on freely behaving rats, a "place cell" fires only when the animal passes through its corresponding "place field"; however, the pattern of firing is unusually variable (Fenton and Muller 1998). This variability could represent additional (nonspatial) information, set by behavioral context (Fenton and Muller 1998). Computational models (Olypher et al. 2002) suggest that variability in place cell firing can be ascribed to relatively slowly (hundreds of milliseconds) fluctuating synaptic inputs, but how this fluctuation survives summation over thousands of synapses is not clear. In our model, balance was maintained by interaction between dendritic and synaptic mechanisms, which allowed information present in input fluctuations and high-frequency oscillations to be detected and passed on by the CA1 neuron.

Several studies have suggested that alteration of the sAHP levels affects maze behavior and learning (Tomabaugh et al. 2005); this is a possible link between cellular excitability in dendrites and changes in behavior. Our specific observations regarding the synergistic action of short-term presynaptic depression and slow, active dendritic currents suggest a testable hypothesis about the involvement of sAHP conductances in the modulation of place cell firing (Fig. 7). Namely, we propose that synergistic interactions between the sAHP and presynaptic plasticity at Schaffer collaterals might be necessary for the efficient encoding of positional and contextual information associated with pyramidal place cell activity (Eichenbaum et al. 1999; Fenton and Muller 1998). In this view, positional information is given by the spatial pattern of synaptic activation at a given moment, whereas the context in which this information is being relayed is provided by the temporal history of synaptic activation and neuronal spiking.

A practical way to test the involvement of dendritic sAHP in the generation of contextual firing could be by monitoring the animal's navigation in the modified T-maze (Wood et al. 2000). In these experiments, the firing pattern of pyramidal neurons with place field on the central stem of a T-maze depended on the route that the animal had taken during the earlier traverse through the maze (either right or left turn). Thus the place-related activity of hippocampal neurons was strongly affected by the context of the ongoing task (Wood et al. 2000). The pharmacological blockade of dendritic sAHP, which, according to our model, would significantly affect the

temporal structure of pyramidal neuron spike time series, could affect the animal's decisions during the navigation in the modified T-maze.

#### GRANTS

This work was supported by the National Science Foundation-sponsored Center for Theoretical Biological Physics (Grants PHY-0216576 and PHY-0225630), the Howard Hughes Medical Institute to T. J. Sejnowski, and the Tauber Fund at Tel-Aviv University to E. Ben-Jacob. V. Volman acknowledges the support of U.S. National Science Foundation I2CAM International Materials Institute Award, Grant DMR-0645461.

#### REFERENCES

- Abbott LF, Varela JA, Sen K, Nelson SB.** Synaptic depression and cortical gain control. *Science* 275: 221–224, 1997.
- Andersen P, Morris R, Amaral D, Bliss T, O'Keefe J.** *The Hippocampus Book*. New York: Oxford, 2007.
- Andreasen M, Lambert JDC.** The excitability of CA1 pyramidal cell dendrites is modulated by a local  $\text{Ca}^{2+}$ -dependent  $\text{K}^{+}$  conductance. *Brain Res* 698: 193–203, 1995.
- Bekkers JM.** Distribution of slow AHP channels on hippocampal CA1 pyramidal neurons. *J Neurophysiol* 83: 1756–1759, 2000.
- Bertram R, Sherman A, Stanley EF.** Single-domain/bound calcium hypothesis of transmitter release and facilitation. *J Neurophysiol* 75: 1919–1931, 1996.
- Buzsaki G.** Theta oscillations in the hippocampus. *Neuron* 33: 325–340, 2002.
- Csicsvari J, Hirase H, Czurko A, Mamiya A, Buzsaki G.** Oscillatory coupling of hippocampal pyramidal cells and interneurons in the behaving rat. *J Neurosci* 19: 274–287, 1999.
- de la Rocha N, Parga N.** Short-term synaptic depression causes a non-monotonic response to correlated stimuli. *J Neurosci* 25: 8416–8431, 2005.
- Dobrunz LE, Huang EP, Stevens CF.** Very short-term plasticity in hippocampal synapses. *Proc Natl Acad Sci USA* 94: 14843–14847, 1997.
- Dobrunz LE, Stevens CF.** Heterogeneity of release probability, facilitation and depletion at central synapses. *Neuron* 18: 995–1008, 1997.
- Eichenbaum H, Dudchenko P, Wood E, Shapiro M, Tanila H.** The hippocampus, memory, and place cells: is it spatial memory or a memory space? *Neuron* 23: 209–226, 1999.
- Fenton AA, Muller RU.** Place cell discharge is extremely variable during individual passes of the rat through the firing field. *Proc Natl Acad Sci USA* 95: 3182–3187, 1998.
- Gabbiani F, Koch C.** Principles of spike train analysis. In: *Methods in Neuronal Modeling*, edited by Koch C, Segev I. Cambridge, MA: MIT Press, 1998, p. 313–360.
- Garcia-Perez E, Wesseling JF.** Augmentation controls the fast rebound from depression at excitatory hippocampal synapses. *J Neurophysiol* 99: 1770–1786, 2008.
- Gasparini S, Magee JC.** State-dependent dendritic computation in hippocampal CA1 pyramidal neurons. *J Neurosci* 26: 2088–2100, 2006.
- Golding NL, Kath WL, Spruston N.** Dichotomy of action-potential back-propagation in CA1 pyramidal neuron dendrites. *J Neurophysiol* 86: 2998–3010, 2001.
- Harris KM, Jensen FE, Tsao B.** 3D structure of dendritic spines and synapses in rat hippocampus (CA1) at postnatal day 15 and adult ages: implications for the maturation of synaptic physiology and long-term potentiation. *J Neurosci* 12: 2685–2705, 1992.
- Hines ML, Carnevale NT.** NEURON: a tool for neuroscientist. *Neuroscientist* 7: 123–135, 2001.
- Hoffman DA, Magee JC, Colbert CM, Johnston D.**  $\text{K}^{+}$  channel regulation of signal propagation in dendrites of hippocampal pyramidal neurons. *Nature* 387: 869–875, 1997.
- Holt GR, Softky WR, Koch C, Douglas RJ.** Comparison of discharge variability in-vitro and in-vivo in cat visual cortex neurons. *J Neurophysiol* 75: 1806–1814, 1996.
- Ishizuka N, Cowan WM, Amaral DG.** A quantitative analysis of the dendritic organization of pyramidal cells in the rat hippocampus. *J Comp Neurol* 362: 17–45, 1995.
- Klyachko VA, Stevens CF.** Excitatory and feed-forward inhibitory hippocampal synapses work synergistically as an adaptive filter of natural spike trains. *PLoS Biol* 4: e207, 2006.
- Larkum ME, Nevian T.** Synaptic clustering by dendritic signalling mechanisms. *Curr Opin Neurobiol* 18: 321–331, 2008.

- Le Ray D, de Sevilla DF, Porto AB, Fuenzalida M, Buno W.** Heterosynaptic metaplastic regulation of synaptic efficacy in CA1 pyramidal neurons of rat hippocampus. *Hippocampus* 14: 1011–1025, 2004.
- Li X, Ascoli GA.** Computational simulation of the input-output relationship in hippocampal pyramidal cells. *J Comput Neurosci* 21: 191–209, 2006.
- Liu G.** Local structural balance and functional interaction of excitatory and inhibitory synapses in hippocampal dendrites. *Nat Neurosci* 7: 373–379, 2004.
- Lorincz A, Notomi T, Tamas G, Shigemoto R, Nusser Z.** Polarized and compartment-dependent distribution of HCN1 in pyramidal cell dendrites. *Nat Neurosci* 5: 1185–1193, 2002.
- Magee JC.** Dendritic hyperpolarization-activated currents modify the integrative properties of hippocampal CA1 pyramidal neurons. *J Neurosci* 18: 7613–7624, 1998.
- Magee JC, Christofi G, Miyakawa H, Christie B, Lasser-Ross N, Johnston D.** Subthreshold synaptic activation of voltage-gated  $\text{Ca}^{2+}$  channels mediates a localized  $\text{Ca}^{2+}$  influx in the dendrites of hippocampal pyramidal neurons. *J Neurophysiol* 74: 1335–1342, 1995.
- Magee JC, Cook EP.** Somatic EPSP amplitude is independent of synapse location in hippocampal pyramidal neurons. *Nat Neurosci* 3: 895–903, 2000.
- Magee JC, Johnston D.** Characterization of single voltage-gated  $\text{Na}^+$  and  $\text{Ca}^{2+}$  channels in apical dendrites of rat CA1 pyramidal neurons. *J Physiol* 487: 67–90, 1995.
- Mainen ZF, Sejnowski TJ.** Modeling active dendritic processes in pyramidal neurons. In: *Methods in Neuronal Modeling*, edited by Koch C, Segev I. Cambridge, MA: MIT Press, 1998, p. 171–209.
- Maletic-Savatic M, Malinow R, Svoboda K.** Rapid dendritic morphogenesis in CA1 hippocampal dendrites induced by synaptic activity. *Science* 283: 1923–1927, 1999.
- Migliore M, Ferrante M, Ascoli GA.** Signal propagation in oblique dendrites of CA1 pyramidal neurons. *J Neurophysiol* 94: 4145–4155, 2005.
- Migliore M, Hoffman DA, Magee JC, Johnston D.** Role of A-type  $\text{K}^+$  conductance in back-propagation of action potentials in the dendrites of hippocampal pyramidal neurons. *J Comput Neurosci* 7: 5–15, 1999.
- Migliore M, Shepherd GM.** Emerging rules for the distributions of active dendritic conductances. *Nat Rev Neurosci* 3: 362–370, 2002.
- Muller RU, Kubie JL, Ranck JB.** Spatial firing patterns of hippocampal complex-spike cells in a fixed environment. *J Neurosci* 7: 1935–1950, 1987.
- Murthy VN, Sejnowski TJ, Stevens CF.** Dynamics of dendritic calcium transients evoked by quantal release at excitatory hippocampal synapses. *Proc Natl Acad Sci USA* 97: 901–906, 2000.
- Nadkarni S, Jung P.** Modeling synaptic transmission of the tripartite synapse. *Phys Biol* 4: 1–9, 2007.
- O’Keefe J, Nadel L.** *The Hippocampus as a Cognitive Map*. Oxford, UK: Clarendon Press, 1978.
- Olypher AV, Lansky P, Fenton AA.** Properties of the extra-positional signal in hippocampal place cell discharge derived from the over-dispersion in location-specific firing. *Neuroscience* 111: 553–566, 2002.
- Pineda JC, Waters RS, Foehring RC.** Specificity in the interaction of HVA  $\text{Ca}^{2+}$  channel types with  $\text{Ca}^{2+}$ -dependent AHPs and firing behavior in neocortical pyramidal neurons. *J Neurophysiol* 79: 2522–2534, 1998.
- Poirazi P, Brannon TM, Mel BW.** Arithmetic of subthreshold synaptic summation in a model CA1 pyramidal cell. *Neuron* 37: 977–987, 2003a.
- Poirazi P, Brannon TM, Mel BW.** Pyramidal neuron as two-layer neural network. *Neuron* 37: 989–999, 2003b.
- Poolos NP, Migliore M, Johnston D.** Pharmacological up-regulation of H-channels reduces the excitability of pyramidal neuron dendrites. *Nat Neurosci* 5: 767–774, 2002.
- Prescott SA, Sejnowski TJ.** Spike-rate coding and spike-time coding are affected oppositely by different adaptation mechanisms. *J Neurosci* 28: 13649–13661, 2008.
- Reyes AD.** Influence of dendritic conductances on the input-output properties of neurons. *Annu Rev Neurosci* 24: 653–675, 2001.
- Sah P, Bekkers JM.** Apical dendritic location of slow afterhyperpolarization current in hippocampal pyramidal neurons: implications for the integration of long-term potentiation. *J Neurosci* 16: 4537–4542, 1996.
- Sah P, Clements JD.** Photolytic manipulation of  $[\text{Ca}^{2+}]_i$  reveals slow kinetics of potassium channels underlying the afterhyperpolarization in hippocampal pyramidal neurons. *J Neurosci* 19: 3657–3664, 1999.
- Salinas E, Sejnowski TJ.** Impact of correlated synaptic input on output firing rate and variability in simple neuronal models. *J Neurosci* 20: 6193–6209, 2000.
- Schwindt PC, Crill WE.** Modification of current transmitted from apical dendrite to soma by blockade of voltage- and  $\text{Ca}^{2+}$ -dependent conductances in rat neocortical pyramidal neurons. *J Neurophysiol* 78: 187–198, 1997.
- Shadlen MN, Newsome WT.** The variable discharge of cortical neurons: implications for connectivity, computation, and information coding. *J Neurosci* 18: 3870–3896, 1998.
- Shah MM, Haylett DG.** Calcium channels involved in the generation of the slow afterhyperpolarization in cultured rat hippocampal pyramidal neurons. *J Neurophysiol* 83: 2554–2561, 2000.
- Softky WR.** Simple codes versus efficient codes. *Curr Opin Neurobiol* 5: 239–247, 1995.
- Softky WR, Koch C.** The highly irregular firing of cortical cells is inconsistent with temporal integration of random EPSPs. *J Neurosci* 13: 334–350, 1993.
- Stemmler M, Koch C.** How voltage-dependent conductances can adapt to maximize the information encoded by neuronal firing rate. *Nat Neurosci* 2: 521–527, 1999.
- Stevens CF, Tsujimoto T.** Estimates for the pool size of releasable quanta at a single central synapse and for the time required to refill the pool. *Proc Natl Acad Sci USA* 92: 846–849, 1995.
- Stuart G, Spruston N, Hausser MH.** *Dendrites*. Oxford, UK: Oxford University Press, 1999.
- Tomabaugh GC, Rowe WB, Rose GM.** The slow afterhyperpolarization in hippocampal CA1 neurons covaries with spatial learning ability in aged Fisher 344 rats. *J Neurosci* 25: 2609–2616, 2005.
- Traub RD, Buhl EH, Gloveli T, Whittington MA.** Fast rhythmic bursting can be induced in layer 2/3 cortical neurons by enhancing persistent  $\text{Na}^+$  conductance or by blocking BK channels. *J Neurophysiol* 89: 909–921, 2003.
- Troyer TW, Miller KD.** Physiological gain leads to high ISI variability in a simple model of a cortical regular spiking cell. *Neural Comput* 9: 971–983, 1997.
- Westenbroek RE, Ahljianian MK, Catterall WA.** Clustering of L-type  $\text{Ca}^{2+}$  channels at the base of major dendrites in hippocampal pyramidal neurons. *Nature* 347: 281–284, 1990.
- Williams SR, Stuart GJ.** Role of dendritic synapse location in the control of action potential output. *Trends Neurosci* 26: 147–152, 2003.
- Wilson CJ, Kawaguchi Y.** The origins of two-state spontaneous membrane potential fluctuations of neostriatal spiny neurons. *J Neurosci* 16: 2397–2410, 1996.
- Wood ER, Dudchenko PA, Robitsek RJ, Eichenbaum H.** Hippocampal neurons encode information about different types of memory episodes occurring in the same location. *J Neurophysiol* 27: 623–633, 2000.
- Yuste R, Denk W.** Dendritic spines as basic units of synaptic integration. *Nature* 375: 682–684, 1995.
- Zucker RS, Regehr WG.** Short-term synaptic plasticity. *Annu Rev Physiol* 64: 355–405, 2002.